

Phenomenology of anomaly-mediated supersymmetry breaking scenarios with non-minimal flavour violation

Benjamin Fuks*

*Institut Pluridisciplinaire Hubert Curien/Département Recherches Subatomiques
Université de Strasbourg/CNRS-IN2P3
23 Rue du Loess, F-67037 Strasbourg, France*

Björn Herrmann†

LAPTh, Université de Savoie, CNRS, B.P. 110, F-74941 Annecy-le-Vieux, France

Michael Klasen‡

*Institut für Theoretische Physik, Universität Münster,
Wilhelm-Klemm-Straße 9, D-48149 Münster, Germany
(Dated: December 26, 2011)*

In minimal anomaly-mediated supersymmetry breaking models, tachyonic sleptons are avoided by introducing a common scalar mass similar to the one introduced in minimal supergravity. This may lead to non-minimal flavour-violating interactions, *e.g.*, in the squark sector. In this paper, we analyze the viable anomaly-mediated supersymmetry breaking parameter space in the light of the latest limits on low-energy observables and LHC searches, complete our analytical calculations of flavour-violating supersymmetric particle production at hadron colliders with those related to gluino production, and study the phenomenological consequences of non-minimal flavour violation in anomaly-mediated supersymmetry breaking scenarios at the LHC. Related cosmological aspects are also briefly discussed.

1. INTRODUCTION

Many alternatives to the Standard Model (SM) of particle physics have been proposed over the last thirty years. Among these, supersymmetry (SUSY), and particularly its minimal version dubbed the Minimal Supersymmetric Standard Model (MSSM) [1, 2], is one of the most popular SM extensions. It consists in a symmetry linking fields with opposite statistics, matching thus a bosonic (fermionic) superpartner with each fermionic (bosonic) SM degree of freedom. As a consequence, it predicts the stabilization of the gap between the electroweak and the Planck scale, gauge coupling unification at high energies, and a lightest supersymmetric particle, which is weakly interacting and stable and thus a good dark matter candidate. Since the superpartners of the SM particles have not yet been observed and in order to remain a viable solution to the hierarchy problem, SUSY must be softly broken at low energy, which makes the SUSY particles massive, with a mass lying in the TeV range. Therefore, SUSY searches at present hadron colliders, such as the Tevatron at Fermilab or the LHC at CERN, are important topics of the current experimental high-energy physics program.

Within the Standard Model, flavour violation in the quark sector arises only through the rotation of the up- and down-type quark interaction eigenstates into the basis of physical mass eigenstates. Four bi-unitary matrices are required to diagonalize the quark Yukawa matrices, which renders the charged-current interactions proportional to the unitary CKM matrix V_{CKM} . In the super-CKM basis [3], the squark interaction eigenstates undergo the same rotations as their quark counterparts, so that their charged-current interactions are also proportional to the CKM matrix. However, in non-minimal flavour-violating supersymmetric theories, the quark and squark fields can be misaligned due to additional sources of flavour violation which are related to the breaking of supersymmetry. As a consequence, this leads to flavour-violating (non-diagonal) entries in the squark mass matrices.

In recent works, we have analysed the cases where such soft terms appear in (non-minimal) supergravity and gauge-mediated SUSY breaking scenarios [4, 5]. In the first case, supersymmetry is broken in a hidden sector and transmitted

*benjamin.fuks@iphc.cnrs.fr

†herrmann@in2p3.fr

‡michael.klasen@uni-muenster.de

to the visible sector of squarks, sleptons, gauginos and gluinos through gravitational interactions. Soft masses for sfermions are induced by direct Kähler interactions, which can in general be flavour non-diagonal [1, 6, 7]. In the second case, the breaking of supersymmetry is mediated to the visible sector via gauge interactions with messenger fields in a flavour-conserving fashion [8–11]. However, it has recently been shown that non-minimal versions of the gauge-mediated SUSY-breaking mechanism can yield important flavour-violation in the squark and slepton sectors [11–13].

When SUSY is broken in a hidden sector, the soft masses also receive contributions from quantum effects due to the superconformal anomaly [14–17]. In this work, we therefore consider this so-called anomaly-mediated SUSY-breaking (AMSB) scenario, where those anomaly-mediated effects are large compared to all other sources of SUSY-breaking, which are subdominant. We extend our previous work on flavour violation [4, 5] by investigating possible non-minimal flavour violation within the AMSB context.

This paper is organized as follows: In Sec. 2, we define anomaly-mediated supersymmetry breaking scenarios and show how non-minimal flavour violation can appear. In Sec. 3 we impose current experimental constraints on the flavour-violating AMSB scenario and perform scans of the parameter space. In addition, experimentally allowed benchmark points are defined. Cross sections for the production of at least one gluino are analytically and numerically computed in Sec. 4. We dedicate Sec. 5 to an analysis of the possible cosmological constraints related to the presence of cold dark matter in our Universe. Our conclusions are presented in Sec. 6.

2. ANOMALY MEDIATION AND FLAVOUR VIOLATION IN THE SQUARK SECTOR

In AMSB scenarios, the soft terms are related to the anomalous dimensions of the different fields and have the feature to be renormalization-group invariant [18, 19]. As a consequence, they are fully determined by the known low-energy gauge and Yukawa couplings and an overall mass scale m_{aux} , the vacuum expectation value of the scalar auxiliary field of the gravitation supermultiplet. This scale is expected to be of the order of the gravitino mass $m_{3/2}$, and we assume in the following, to simplify, $m_{3/2} = m_{\text{aux}}$. Consequently, the model is highly predictive, with fixed mass ratios and distinctive signatures [16, 20–23]. Among all the predictions, one finds, however, tachyonic sleptons. This problem must be cured in order to have a phenomenologically viable model. Several solutions have been proposed [14, 17, 24–33], and we adopt here the phenomenological approach of assuming non-negligible contributions to the scalar soft masses, induced, *e.g.*, by supergravity, which makes their square positive at the weak scale. However, in this case, solving the tachyonic sfermion mass problem can also introduce non-minimal flavour violation in the theory, through possible non-diagonal flavour-violating soft mass terms.

The squark mass matrices are written, in the super-CKM basis, as

$$M_{\tilde{q}}^2 = \left(\begin{array}{ccc|ccc} M_{L_{q_1}}^2 & \Delta_{LL}^{q_1 q_2} & \Delta_{LL}^{q_1 q_3} & m_{q_1} X_{q_1} & \Delta_{LR}^{q_1 q_2} & \Delta_{LR}^{q_1 q_3} \\ \Delta_{LL}^{q_1 q_2*} & M_{L_{q_2}}^2 & \Delta_{LL}^{q_2 q_3} & \Delta_{RL}^{q_1 q_2*} & m_{q_2} X_{q_2} & \Delta_{RL}^{q_2 q_3} \\ \Delta_{LL}^{q_1 q_3*} & \Delta_{LL}^{q_2 q_3*} & M_{L_{q_3}}^2 & \Delta_{RL}^{q_1 q_3*} & \Delta_{RL}^{q_2 q_3*} & m_{q_3} X_{q_3} \\ \hline m_{q_1} X_{q_1}^* & \Delta_{RL}^{q_1 q_2} & \Delta_{RL}^{q_1 q_3} & M_{R_{q_1}}^2 & \Delta_{RR}^{q_1 q_2} & \Delta_{RR}^{q_1 q_3} \\ \Delta_{LR}^{q_1 q_2*} & m_{q_2} X_{q_2}^* & \Delta_{RL}^{q_2 q_3} & \Delta_{RR}^{q_1 q_2*} & M_{R_{q_2}}^2 & \Delta_{RR}^{q_2 q_3} \\ \Delta_{LR}^{q_1 q_3*} & \Delta_{LR}^{q_2 q_3*} & m_{q_3} X_{q_3}^* & \Delta_{RR}^{q_1 q_3*} & \Delta_{RR}^{q_2 q_3*} & M_{R_{q_3}}^2 \end{array} \right), \quad (2.1)$$

where the flavour-diagonal elements are given by

$$\begin{aligned} M_{L_{q_i}}^2 &= M_{\tilde{Q}_i}^2 + m_{q_i}^2 + \cos 2\beta m_Z^2 (T_q^3 - e_q s_W^2), \\ M_{R_{q_i}}^2 &= M_{\tilde{U}_i}^2 + m_{q_i}^2 + \cos 2\beta m_Z^2 e_q s_W^2 \quad \text{for up-type squarks,} \\ M_{R_{q_i}}^2 &= M_{\tilde{D}_i}^2 + m_{q_i}^2 + \cos 2\beta m_Z^2 e_q s_W^2 \quad \text{for down-type squarks,} \\ X_{q_i} &= A_{q_i}^* - \mu \begin{cases} \cot \beta & \text{for up-type squarks,} \\ \tan \beta & \text{for down-type squarks.} \end{cases} \end{aligned} \quad (2.2)$$

The weak isospin quantum numbers are $T_q^3 = \pm 1/2$ for left-handed up-type and down-type (s)quarks, their fractional electromagnetic charge is denoted by e_q , and m_{q_i} is the mass of the quark q_i , i being the flavour index, *i.e.*, $d_1 = d$, $d_2 = s$, $d_3 = b$, $u_1 = u$, $u_2 = c$, and $u_3 = t$. In addition, m_Z is the Z -boson mass, and s_W is the sine of the electroweak mixing angle. The soft supersymmetry-breaking mass terms are $M_{\tilde{Q}_i}^2$ and $M_{\{\tilde{U}_i, \tilde{D}_i\}}$ for the left-handed and right-handed squarks, while the quantities A_{q_i} are the trilinear couplings between the Higgs bosons and the scalar SUSY particles. In the Higgs sector, μ denotes the off-diagonal superpotential Higgs mass parameter, and $\tan \beta = v_u/v_d$ is

the ratio of vacuum expectation values of the two Higgs doublets. In our phenomenological approach, the off-diagonal parameters $\Delta_{ab}^{qq'}$ are arbitrary and can be normalized to the diagonal entries according to [34]

$$\Delta_{ab}^{q_i q_j} = \lambda_{ab}^{q_i q_j} M_{q_i} M_{q_j} . \quad (2.3)$$

Additional sources of quark flavour violation are then parameterized through the 21 dimensionless (possibly complex) new variables $\lambda_{ab}^{q_i q_j}$, since due to $SU(2)$ gauge invariance, the $\Delta_{LL}^{qq'}$ elements of the up- and down-type squark squared mass matrices are related to each other,

$$M_{\tilde{u},LL}^2 = V_{\text{CKM}} M_{\tilde{d},LL}^2 V_{\text{CKM}}^\dagger , \quad (2.4)$$

as are the associated λ -parameters. This equation shows that both squark mass matrices cannot be simultaneously diagonal (without neglecting the CKM matrix). The diagonalization of the mass matrices $M_{\tilde{u}}^2$ and $M_{\tilde{d}}^2$ requires the introduction of two 6×6 matrices R^u and R^d ,

$$\text{diag}(m_{\tilde{u}_1}^2, \dots, m_{\tilde{u}_6}^2) = R^u M_{\tilde{u}}^2 R^{u\dagger} \quad \text{and} \quad \text{diag}(m_{\tilde{d}_1}^2, \dots, m_{\tilde{d}_6}^2) = R^d M_{\tilde{d}}^2 R^{d\dagger} , \quad (2.5)$$

where by convention the masses are ordered increasingly, $m_{\tilde{q}_1} < \dots < m_{\tilde{q}_6}$. These mixing matrices relate the physical mass eigenbasis to the interaction eigenbasis through

$$(\tilde{u}_1, \tilde{u}_2, \tilde{u}_3, \tilde{u}_4, \tilde{u}_5, \tilde{u}_6)^t = R^u (\tilde{u}_L, \tilde{c}_L, \tilde{t}_L, \tilde{u}_R, \tilde{c}_R, \tilde{t}_R)^t \quad \text{and} \quad (\tilde{d}_1, \tilde{d}_2, \tilde{d}_3, \tilde{d}_4, \tilde{d}_5, \tilde{d}_6)^t = R^d (\tilde{d}_L, \tilde{s}_L, \tilde{b}_L, \tilde{d}_R, \tilde{s}_R, \tilde{b}_R)^t . \quad (2.6)$$

Recently, it has been shown that (minimal) AMSB scenarios with an additional $U(1)$ symmetry satisfy the requirements of the Minimal Flavour Violation principles [35]. In this case, the λ -parameters are not free and directly dictated from the flavour structure of the CKM matrix. In our approach, we are going beyond this scheme, keeping the flavour-violation parameters independent.

3. EXPERIMENTAL CONSTRAINTS ON AMSB MODELS

3.1. Constraints

In this Section, we discuss the most relevant experimental measurements that can be used to constrain the parameter space of the MSSM. Apart from direct searches for superpartners at collider experiments, and particularly the recent results of the ATLAS and CMS experiments at the LHC [36, 37], numerous low-energy and electroweak precision measurements [38, 39] constrain masses and mixings of the superpartners. They can often impose stronger limits on the flavour-violating entries introduced in Sec. 2.

Extensive studies of the kaon sector, B - and D -meson oscillations, rare decays, and electric dipole moments suggest that only flavour mixing involving the second and third generations of squarks can be substantial, and this only in the left-left and right-right chiral sectors, which mix the superpartners of the left-handed and right-handed quarks [34, 40–42]. For this reason, we restrict ourselves to the simpler scenario where only the flavour-mixing parameters related to the second and third generations and non mixing squark chiralities can be non-vanishing,

$$\lambda_L \equiv \lambda_{LL}^{ct}, \quad \lambda_u \equiv \lambda_{RR}^{ct} \quad \text{and} \quad \lambda_d \equiv \lambda_{RR}^{sb} . \quad (3.1)$$

The parameter related to the mixing among second and third generation down-type squarks λ_{LL}^{sb} is not a free parameter of our simplified model, since it is connected to λ_L through Eq. (2.4).

The measurement of the rare $b \rightarrow s\gamma$ decay represents one of the most stringent constraints on these squark mixings. The inclusive branching ratio is determined to be

$$\text{BR}(b \rightarrow s\gamma) = (3.55 \pm 0.26_{\text{exp}} \pm 0.23_{\text{theo}}) \times 10^{-4} \quad (3.2)$$

from BABAR, BELLE, and CLEO data [39]. For the theoretical error estimate, we refer to the discussion in Refs. [43, 44]. Squark diagrams contribute already at the one-loop level, as do the SM particles. As a consequence, this measurement can lead to strong constraints on the squark masses and couplings, especially on the λ_L parameter of the left-left chiral sector, since the lightest neutralinos and charginos appearing in the loops are mostly winos coupling to the left-handed components of the squark mass-eigenstates. The same arguments apply to the $b \rightarrow s\mu^+\mu^-$ branching fraction, experimentally measured as [39]

$$\text{BR}(b \rightarrow s\mu^+\mu^-) = (2.23 \pm 0.98_{\text{exp}} \pm 0.11_{\text{theo}}) \times 10^{-6} , \quad (3.3)$$

the associated theoretical uncertainties being computed in Ref. [45], or to the B_s^0 -meson branching fractions to a muon pair, recently bounded from above by the CMS and LHCb experiments [46],

$$\text{BR}(B_s^0 \rightarrow \mu^+ \mu^-) < 1.1 \times 10^{-8} , \quad (3.4)$$

at 95% confidence level, which is, however, still about four or five times larger than the SM expectation.

Also, the $B_s^0 - \bar{B}_s^0$ oscillations, which have been recently observed, directly probe the mixing between squarks of the second and third generations. Since NMFV contributions arise at the same loop level as the SM ones, this observable can again be sensitive to non-vanishing λ -parameters. Hence, the measured mass difference [39]

$$\Delta M_{B_s^0} = (17.78 \pm 0.12_{\text{exp}} \pm 3.3_{\text{theo}}) \text{ ps}^{-1} , \quad (3.5)$$

where the theoretical uncertainty of 3.3 ps^{-1} at the 95% confidence level has been derived in Ref. [47], allows to constrain the magnitude of the above-mentioned flavour-violating parameters.

Another important consequence of NMFV mixing in the squark sector is a large splitting between squark mass eigenvalues. This influences the Z - and W -boson self-energies at zero momentum, contributing hence to the electroweak ρ -parameter

$$\Delta\rho = \frac{\Sigma_Z(0)}{m_Z^2} - \frac{\Sigma_W(0)}{m_W^2} = \alpha(m_Z)T = (2.36 \pm 8.65) \times 10^{-4} , \quad (3.6)$$

the experimental value arising from combined fits of the Z -boson mass, width, and pole asymmetry as well as of the masses of the W -boson and the top quark [38].

Furthermore, recent measurements of the anomalous magnetic moment of the muon $(g-2)_\mu$ indicate a discrepancy of about 3σ between the data and the Standard Model predictions [38],

$$a_\mu^{\text{exp}} - a_\mu^{\text{SM}} = (25.5 \pm 7.98) \times 10^{-10} \quad \text{with} \quad a_\mu \equiv (g-2)_\mu/2. \quad (3.7)$$

This gap could be explained by new physics. In the case of supersymmetric scenarios, the leading contributions, depending on the smuon, sneutrino, chargino and neutralino masses, have been found to be proportional to the sign of the μ -parameter [48]. Since negative values would then increase the discrepancy, we limit ourselves to positive values of μ . Moreover, since squarks contribute only at the two-loop level, the dependence on flavour violation in the squark sector is expected to be considerably reduced. Finally, from direct searches of the Higgs boson, we ask for the mass of the lightest Higgs-boson to fulfil

$$111 \text{ GeV} \lesssim m_h \lesssim 130 \text{ GeV} . \quad (3.8)$$

The lower bound is based on the exclusion limit of $m_h < 114.4 \text{ GeV}$ from LEP [38], after accounting for a theoretical uncertainty of about 3 GeV [49], whilst the upper bound corresponds to the non-observation of a Higgs boson by the ATLAS and CMS experiments [50, 51]. For a restricted set of universal scalar mass m_0 , introduced to solve the tachyonic slepton problem, smaller than a few TeV, the upper bound is almost always satisfied. Considering quantum corrections, the Higgs mass m_h depends on the squark masses, and thus on the flavour-violating entries in the associated mass matrices.

3.2. Analysis of the parameter space related to AMSB scenarios with non-minimal flavour violation

In order to study the phenomenology of AMSB models including non-minimal flavour violation, we have scanned over the parameter space of the model, generalizing the squark mass matrices by including the three flavour-violation parameters presented in Eq. (3.1). Our procedure starts at a high-energy scale, where we define our input parameters as the gravitino mass $m_{3/2}$, the universal scalar mass m_0 introduced to solve the tachyonic slepton problem, the ratio of the two neutral Higgs field vacuum expectation values $\tan\beta = v_u/v_d$, and the sign of the Higgs mixing parameter $\text{sgn}(\mu)$. The soft supersymmetry-breaking terms at the electroweak scale are then obtained through renormalization group running using the `SPheno` package version 3.0 [49], which solves the renormalization group equations numerically to two-loop order and extracts the particle spectrum and mixings at the electroweak scale at the one-loop level for the matter and gauge sectors and at the two-loop level for the Higgs sector. It also computes the electroweak precision and low-energy observables presented in Sec. 3.1.

For the numerical values of the Standard Model parameters, we fix the top quark pole mass to $m_{\text{top}}^{\text{pole}} = 173.2 \text{ GeV}$ [52], the bottom quark mass to $m_b(m_b) = 4.2 \text{ GeV}$ and the Z -boson mass to $m_Z = 91.1876 \text{ GeV}$. The Fermi constant has been taken as $G_F = 1.16637 \times 10^{-5} \text{ GeV}^{-2}$, and the strong and electromagnetic coupling constants at

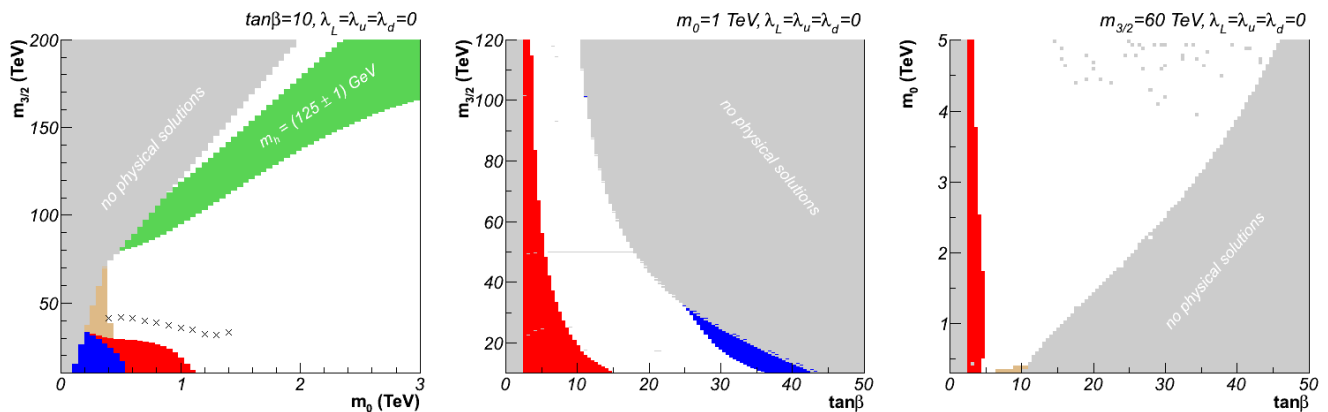


FIG. 1: Scans of the minimal AMSB parameter space, where all flavour-violating parameters, apart from the CKM matrix, vanish, in the $(m_0, m_{3/2})$ plane at fixed $\tan\beta = 10$ (left panel), in the $(\tan\beta, m_{3/2})$ plane at fixed $m_0 = 1$ TeV (central panel) and in the $(\tan\beta, m_0)$ plane at fixed $m_{3/2} = 60$ TeV (right panel). We show regions where there is no physical solution to the renormalization group equations (grey), or which are excluded by the constraints related to the $b \rightarrow s\gamma$ branching ratio (blue) and the Higgs mass (red). The regions, where the agreement between theory and experiment for the anomalous magnetic moment of the muon is restored, are presented in beige. On the left panel, we also indicate the region where the mass of the lightest Higgs boson is close to 125 GeV (green) and the exclusion limit obtained (crosses) from the reinterpretation of the LHC results on supersymmetric particle searches in the context of AMSB scenarios (see Ref. [53]).

the Z -pole as $\alpha_s(m_Z) = 0.1176$ and $\alpha(m_Z)^{-1} = 127.934$. At this stage, the only source of flavour violation lies within the CKM-matrix, which is calculated using the Wolfenstein parametrization. The corresponding four free parameters are set to $\lambda^{(\text{CKM})} = 0.2272$, $A^{(\text{CKM})} = 0.818$, $\bar{\rho}^{(\text{CKM})} = 0.221$, and $\bar{\eta}^{(\text{CKM})} = 0.34$ [38].

In Fig. 1, we present typical scans of the *minimal* AMSB parameter space, *i.e.*, when flavour-violation is induced by the CKM-matrix alone and all λ -parameters vanish. We show the examples of the $(m_0, m_{3/2})$ plane at fixed $\tan\beta = 10$ (left panel), the $(\tan\beta, m_{3/2})$ plane at fixed $m_0 = 1$ TeV (central panel) as well as the $(\tan\beta, m_0)$ plane at fixed $m_{3/2} = 60$ TeV (right panel). All experimental limits described in Sec. 3.1 are imposed at the 2σ -level. We observe that the low-mass regions with a relatively small m_0 , attractive from a collider point of view, are strongly disfavoured by both the measurements of the $b \rightarrow s\gamma$ branching ratio and the too low predicted mass for the lightest Higgs boson. The latter also excludes small values of $\tan\beta$ for a large range of m_0 and $m_{3/2}$ masses. In addition, a significant part of the regions where the predicted value for the $b \rightarrow s\gamma$ branching ratio lies outside the 2σ -range deduced from Eq. (3.2) is also excluded by the constraints associated to the $b \rightarrow s\mu^+\mu^-$ branching ratio. Therefore, these regions have not been shown on Fig. 1, for clarity. Predictions for the other considered B -physics observables, $\Delta M_{B_s^0}$ and the branching ratio $B_s^0 \rightarrow \mu^+\mu^-$, are mostly compatible with data and hence absent from the figure, as is the computed value for the $\Delta\rho$ parameter. This quantity only restricts the parameter space at very heavy masses, which lie outside the mass range presented in the figures.

On the left panel of Fig. 1, we also show the exclusion limits on the parameter space of AMSB scenarios obtained from a reinterpretation of the results of the direct searches for superparticles at the LHC in the AMSB context [53], as well as the region where the mass of the lightest Higgs boson is close to 125 GeV, a value favoured by the recent observations of the ATLAS and CMS experiments [50, 51]. However, in the absence of a confirmed signal for a Higgs boson in that mass range, we do not consider this last limit for our analysis in the sequel.

The size of the regions, where the gap between the data and the predictions for the anomalous magnetic moment of the muon a_μ is closed, is relatively small. Moreover, a significant fraction of it is excluded by the $b \rightarrow s\gamma$ constraint, as it has also been found in Refs. [35, 54]. Hence, a possible explanation of the discrepancy between theory and data for this observable by contributions related to AMSB scenarios is rather difficult. However, the dominant supersymmetric contributions to a_μ highly depend on the slepton masses, entering into the theoretical calculation already at the one-loop level. Since in the context of AMSB scenarios, any prediction associated to the slepton sector is tightly linked to the employed solution to solve the tachyonic slepton problem, we choose to relax the constraint associated to the anomalous magnetic moment of the muon. This is also motivated by the fact that non-minimal flavour violation in the squark sector, *i.e.*, the scope of this paper, contributes subdominantly, at the two-loop level, to a_μ , so that it becomes almost independent of the λ -parameters as it was already noticed in the discussions of Refs. [4, 5].

We now turn to non-minimal flavour violation in AMSB scenarios, where non-vanishing λ -parameters can arise, *e.g.*, from non-trivial Kähler interactions as in supergravity. In our phenomenological approach, we introduce non-minimal

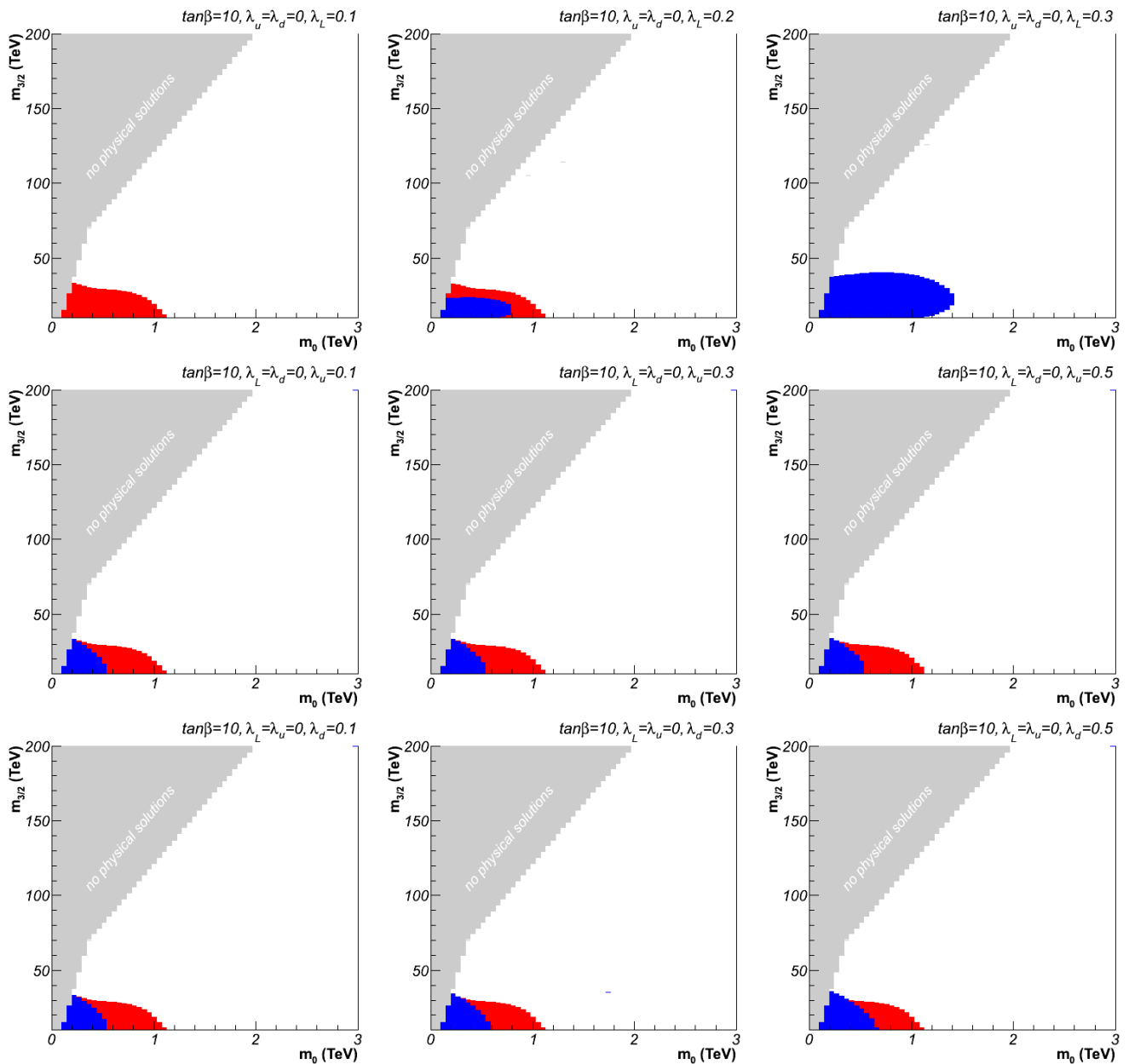


FIG. 2: Typical scans of NMFV AMSB scenarios in the $(m_0, m_{3/2})$ plane with a fixed value of $\tan\beta = 10$. The sign of the μ -parameter is chosen positive and we present the results for different values of the NMFV-parameters λ_L (upper panels), λ_u (central panels) and λ_d (lower panels). We show regions excluded due to the absence of physical solutions to the renormalization group equations (grey), by the constraints associated to the $b \rightarrow s\gamma$ branching ratio (blue) and the Higgs mass (red).

flavour violation at the weak scale, generalizing the squark mass matrices by introducing the three parameters defined in Eq. (3.1). We use again the `SPheno 3.0` program to diagonalize the squark sector and compute the flavour and weak observables presented in Sec. 3.1. In Figs. 2 and 3, we depict the impact of the considered NMFV parameters on these observables, showing the associated constraints on the non-minimal AMSB parameter space. We impose the above-mentioned limit for the Higgs-boson mass, *i.e.*, $m_h \gtrsim 111$ GeV (see the discussion in Section 3.1), as well as all the other constraints at the 2σ confidence level. We present different typical AMSB planes for different values of the flavour-violating λ -parameters, keeping only the most constraining observables for clarity and neglecting the anomalous magnetic moment of the muon for the reasons mentioned above.

Typical scans in the $(m_0, m_{3/2})$ planes of the AMSB parameter space are shown in Fig. 2. We use a fixed value of $\tan\beta = 10$ and choose a positive sign for the μ -parameter. Comparing with the corresponding minimal AMSB

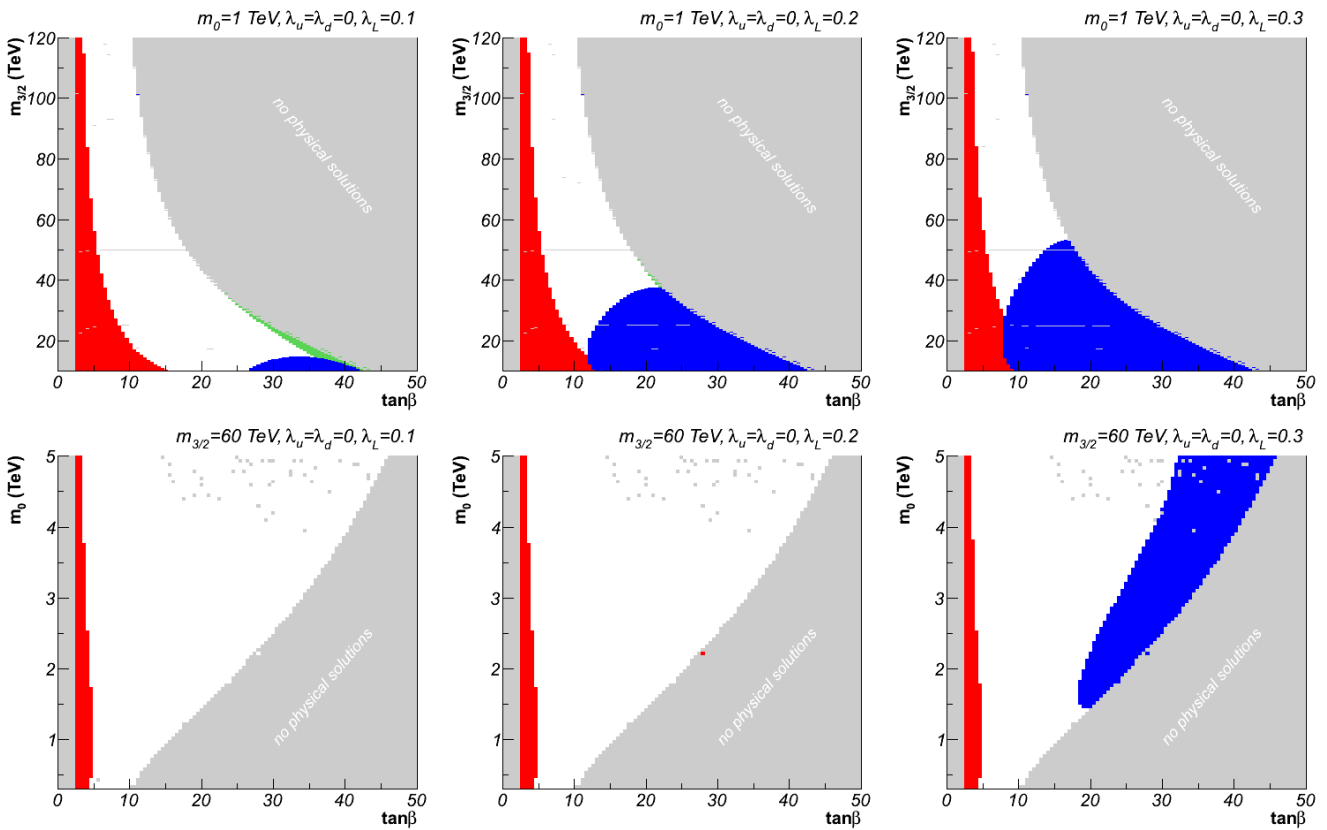


FIG. 3: Scans of NMFV AMSB scenarios in the $(\tan \beta, m_{3/2})$ plane with a fixed value of $m_0 = 1$ TeV (upper panels) and in the $(\tan \beta, m_0)$ plane with a fixed value of $m_{3/2} = 60$ TeV (lower panels). The sign of the μ -parameter is chosen positive and we present the results for different values of the NMFV-parameter λ_L . We show regions excluded due to the absence of physical solutions to the renormalization group equations (grey), by the constraints associated to the $b \rightarrow s\gamma$ branching ratio (blue), the B_s^0 -meson branching to a muon pair $\text{BR}(B_s^0 \rightarrow \mu^+ \mu^-)$ (green) and the lightest Higgs-boson mass (red).

results (left panel of Fig. 1), we find that the most sensitive observable is the $b \rightarrow s\gamma$ branching ratio, which directly probes squark mixing in the left-left chiral sector, *i.e.*, the λ_L -parameter. This strong dependence is due to squark and neutralino-chargino loops, involving $SU(2)_L$ interactions between squarks, quarks and neutralinos or charginos, proportional to the squark mixing matrices R^u and R^d (see Eq. (4.5) below). This also explains the less pronounced sensitivity to NMFV mixing in the right-right chiral sectors (λ_u and λ_d), where the results do not show any strong dependence on the λ -parameters. At intermediate values of $\lambda_L \sim 0.1$, the interplay between squark masses and mixings is such that almost all the parameter space accessible by renormalization group running remains allowed by the $b \rightarrow s\gamma$ branching ratio compared to the minimal results of Fig. 1. Similar conclusions hold for the $b \rightarrow s\mu\mu$ branching ratio, not presented on the figures for clarity. The other considered observables, *e.g.*, the constraint on the lightest Higgs boson mass, are barely sensitive to non-minimal flavour violation, as the dependence on the squark sector is subdominant.

In Fig. 3, we investigate the dependence of the predictions for weak and flavour observables on $\tan \beta$. We first fix the universal scalar mass m_0 to 1 TeV and scan over the $(\tan \beta, m_{3/2})$ plane. Secondly, we fix the gravitino mass $m_{3/2}$ to 60 TeV and scan over the $(\tan \beta, m_0)$ plane. In both cases, the sign of the μ -parameter is again chosen to be positive. As for the analysis in Fig. 2, the most sensitive observables to non-minimal flavour violation are the $b \rightarrow s\gamma$ and $b \rightarrow s\mu\mu$ branching ratios. Since the constraints related to the second decay are weaker and overlapping with those of the first, they are again omitted from the figures. The regions of the parameter space excluded by the constraints associated to the $b \rightarrow s\gamma$ branching ratio increase with the values of the flavour-violating parameter λ_L . For small values, squark mixings and mass effects compensate, which leaves again almost all the parameter space open. In fact, the exclusion contours related to the $b \rightarrow s\gamma$ branching ratio even vanish, when λ_L increases slightly. Such contours reappear only at much larger λ_L values. As a consequence, for $\tan \beta \gtrsim 20$, possible flavour violating entries in the squark mass matrices are reduced to be rather modest, *i.e.*, $\lambda_L \lesssim 0.15$. On the other hand, very low

TABLE I: Three AMSB benchmark scenarios allowing for sizeable flavour-violating entries in the squark mass matrices with respect to the second and third generation mixing in the left-left and/or the right-right chiral squark sectors. The SPS9 scenario is also presented for comparison. We indicate the SUSY-breaking parameters at the high scale and the resulting masses at low energy (after renormalization group running) for the gluino, the lightest squarks and sleptons, the two lightest neutralinos, the lightest chargino, and the lightest Higgs-boson. The values are presented assuming constrained minimal flavour-violation, *i.e.*, when $\lambda_L = \lambda_u = \lambda_d = 0$.

	$m_{3/2}[\text{TeV}]$	$m_0[\text{TeV}]$	$\tan\beta$	$\text{sgn}(\mu)$	[GeV]								
					$m_{\tilde{g}}$	$m_{\tilde{u}_1}$	$m_{\tilde{d}_1}$	$m_{\tilde{\ell}_1}$	$m_{\tilde{\nu}_1}$	$m_{\tilde{\chi}_1^0}$	$m_{\tilde{\chi}_2^0}$	$m_{\tilde{\chi}_1^\pm}$	m_{h^0}
SPS9	60	0.45	10	+	1321.5	950.0	1133.3	339.7	364.1	173.5	542.2	173.7	118.4
I	60	1	10	+	1352.3	1087.6	1332.9	947.8	957.5	174.5	547.2	174.7	116.9
II	60	2	20	+	1394.2	1469.7	1865.4	1906.4	1940.6	176.4	550.8	176.6	118.7
III	60	3	30	+	1417.0	1950.7	2460.7	2743.1	2860.6	176.9	552.6	177.1	121.0

values of $\tan\beta$ are excluded by the bounds on the lightest Higgs boson mass for all values of λ_L . It is also interesting to remark that the predictions for the $\text{BR}(B_s^0 \rightarrow \mu^+ \mu^-)$ observable lie above the current experimental bounds of Eq. (3.4) in the rather large $\tan\beta$ region, for moderate values of the mixing parameter of the left-left chiral sector ($\lambda_L \in [0.1 - 0.2]$) and for relatively light gravitino and universal scalar masses.

Let us finally note that the results for non-minimal flavour violation in the right-right chiral sector are unchanged with respect to the minimal case shown in Fig. 1, and we subsequently do not present the corresponding figures.

3.3. Benchmark scenarios for non-minimally flavour violating AMSB scenarios

Inspecting the various AMSB planes presented in Sec. 3.2, we select three benchmark scenarios allowed by the present low-energy and electroweak precision constraints, which permit a sizeable mixing between second and third generation squarks and which are collider-friendly in the sense that one or several superpartners could be produced with a large rate at the LHC. This means that at least some of the superpartners should not be too heavy. The chosen benchmark points are presented in Tab. I, together with the SPS9 benchmark point [55] which is shown as a reference. As a generic feature for all the four points, the gravitino mass is taken as $m_{3/2} = 60$ TeV and the sign of the off-diagonal Higgs mixing parameter is positive, for the reasons discussed in Sec. 3.1. Due to the renormalization group running invariance of the gaugino mass parameters M_1 , M_2 and M_3 , the dependence of the masses of the gluino, the two lightest neutralinos and the lightest chargino, all mainly gaugino-like, on m_0 and $\tan\beta$ is reduced and subdominant. Therefore, they are roughly identical for all scenarios, with $m_{\tilde{g}} \sim 1300 - 1400$ GeV, $m_{\tilde{\chi}_1^0} \sim m_{\tilde{\chi}_1^\pm} \sim 175$ GeV, and $m_{\tilde{\chi}_2^0} \sim 550$ GeV. In contrast, the scalar spectrum is quite different.

The point SPS9 presents a low value of $\tan\beta = 10$ as well as a relatively low sfermion mass parameter $m_0 = 450$ GeV. Therefore, the masses of the colour-neutral scalar partners of the SM fermions remain rather moderate, while the squark masses are comparable to the gluino mass. The lightest Higgs boson mass, $m_{h^0} = 118.4$ GeV, lies well within the limit of Eq. (3.8). Our first benchmark point I differs very little from the SPS9 scenario, with a moderately larger universal scalar mass $m_0 = 1$ TeV. As a consequence, the slepton masses are of about 1 TeV, while the squarks are only slightly heavier. Even if the lightest Higgs boson mass is now a bit smaller, it lies still well above the excluded limit.

The points II and III feature higher values for $\tan\beta = 20$ and 30, respectively. In order to be able to solve the renormalization group equations, one must then either decrease the value of $m_{3/2}$ or increase the value of m_0 , as it can be seen from Fig. 1. Since the first possibility does not allow for large NMFV mixing in the squark sector due to the $b \rightarrow s\gamma$ branching ratio constraint, we adopt the second choice and fix the universal scalar mass to $m_0 = 2$ TeV and 3 TeV for the scenarios II and III, respectively. Sfermions are therefore considerably heavier, with masses lying in the 2 – 3 TeV range. The mass of the lightest Higgs boson lies still above the constraint of Eq. (3.8). Let us note that for these two scenarios, the squarks are lighter than the sleptons, which may lead to non-leptonic supersymmetric cascade decays as a typical collider signature.

Starting from the minimally flavour-violating scenarios I, II, and III, we now include possible non-minimal flavour-violation in the squark sector, *i.e.*, we allow for λ_L , λ_u and λ_d to be non-vanishing. However, we restrain ourselves to the cases where the off-diagonal entries in the squark mass matrices do not exceed the diagonal ones, *i.e.*, $|\lambda| < 1$. We investigate in Fig. 4 the dependence of the predictions for the observables $\text{BR}(b \rightarrow s\gamma)$, $\Delta M_{B_s^0}$, $\text{BR}(b \rightarrow s\mu\mu)$ and $\text{BR}(B_s^0 \rightarrow \mu^+ \mu^-)$ on the NMFV-parameters and derive the allowed ranges for λ_L , λ_u , and λ_d under the assumption of a single non-vanishing parameter. We present in the (λ_L, λ_u) (upper panel) and (λ_L, λ_d) (lower panel) planes the

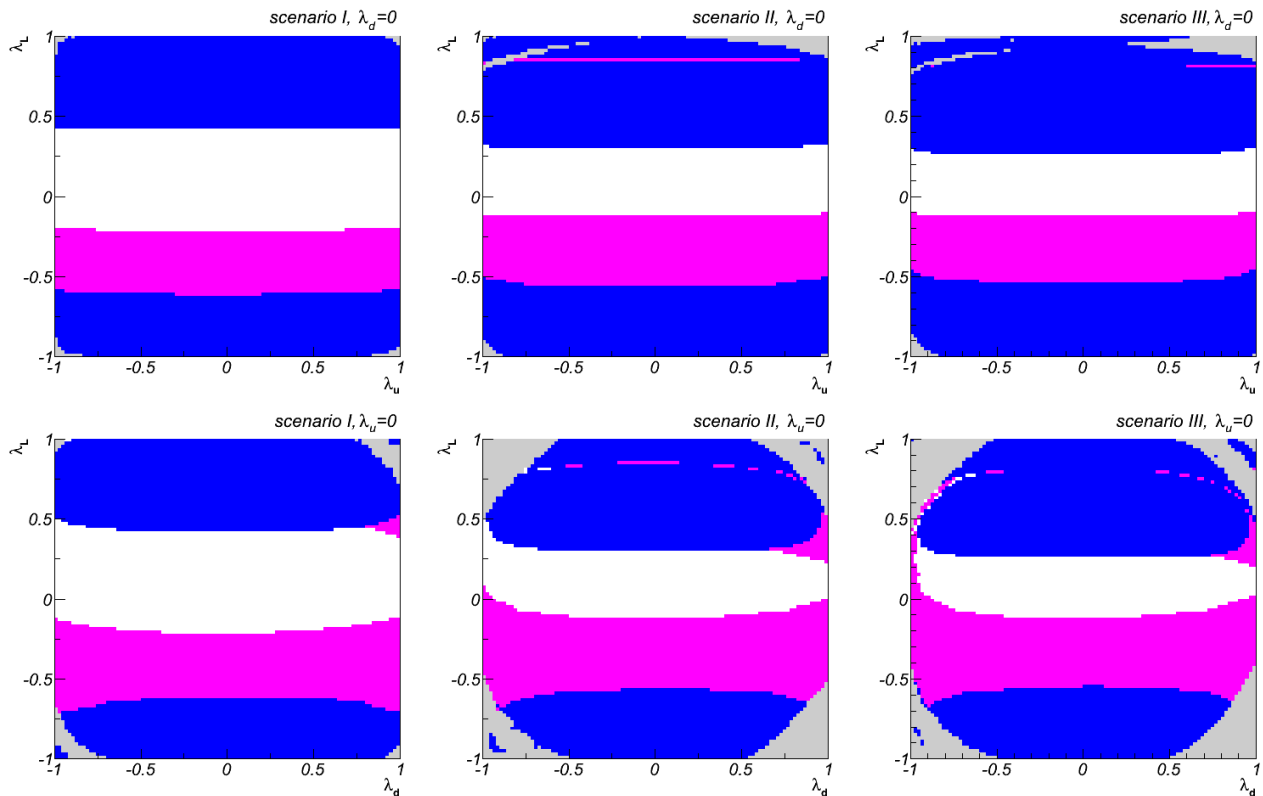


FIG. 4: (λ_L, λ_u) (upper panel) and (λ_L, λ_d) (lower panel) planes for the three scenarios I (left), II (center) and III (right) presented in Tab. I. We show regions excluded due to the absence of physical solutions for the diagonalization of the mass matrices at the one-loop level (grey), the constraints associated to the $b \rightarrow s\gamma$ branching ratio (blue) and the B -meson mass difference $\Delta M_{B_s^0}$ (purple).

regions excluded after confronting the AMSB predictions to the observed experimental values. The regions where the mass matrices, at the one-loop level, cannot be diagonalized are indicated in grey.

As can be seen, strong constraints are imposed by the decay $b \rightarrow s\gamma$ and the meson mass difference $\Delta M_{B_s^0}$. For all scenarios, while the $b \rightarrow s\gamma$ branching ratio data forbid too large (absolute) values for the λ_L parameter, $B_s^0 - \bar{B}_s^0$ oscillations almost completely forbid negative values. Contrary, in the right-right chiral sector non-minimal flavour violation is left rather unconstrained, if not too large values of λ_L are assumed. Hence, in the case of the point I and assuming a single dominant λ -parameter hypothesis, *i.e.*, allowing only one single non-vanishing off diagonal element in the squark mass matrices, NMFV in the left-left chiral sector is constrained to $-0.22 \lesssim \lambda_L \lesssim 0.42$ (with the two other parameters being set to $\lambda_u = \lambda_d = 0$). On the other hand, assuming non-minimal flavour violation only in the right-right chiral sector ($\lambda_L = 0$), we observe that both the λ_u and λ_d parameters are left almost unconstrained, leading to possible large flavour violating effects.

Similarly, regarding scenario II and accounting for all constraints, the left-left chiral sector NMFV parameter is restricted to $-0.12 \lesssim \lambda_L \lesssim 0.3$ in the $\lambda_u = \lambda_d = 0$ case, and λ_u is left unconstrained in the $\lambda_L = 0$ case. However, the higher value of $\tan\beta = 20$ renders the $\Delta M_{B_s^0}$ observable sensitive to very high (absolute) values of λ_d , due to enhanced Yukawa couplings with the down-type (s)quark sector. This yields the constraint $-0.92 \lesssim \lambda_d \lesssim 0.96$ if the flavour-violation is assumed to be located only in the down-type squark right-right chiral sector.

This effect on $\Delta M_{B_s^0}$ is a bit more pronounced for the third scenario, with its large value of $\tan\beta = 30$, yielding moderate constraints for scenarios with non-minimal flavour-violation in the right-right down-type squark chiral sector ($-0.88 \lesssim \lambda_d \lesssim 0.9$). For NMFV in the left-left chiral sector, with $\lambda_u = \lambda_d = 0$, one observes that the allowed range for λ_L is now severely restricted, as for the second scenario, to $-0.12 \lesssim \lambda_L \lesssim 0.26$. All the results are summarized in Tab. II.

For scenario I, we show in Fig. 5 the dependence of the mass eigenvalues and the flavour decomposition of selected down-type squarks on the NMFV-parameter λ_d , as an example, which induces a $\tilde{b}_R - \tilde{s}_R$ mixing. With increasing off-diagonal elements in the squark mass matrix, the resulting splitting of the physical mass eigenvalues becomes more

TABLE II: Ranges for the flavour-violating parameters λ_L , λ_u and λ_d compatible with the low-energy and electroweak precision observables in the case of our three reference scenarios of Tab. I. The limits are given under the assumption of a single NMFV parameter, *i.e.*, where only one single parameter is allowed to vary, the other being set to zero. If no value is indicated, the whole explored range of $-1 < \lambda_{u,d} < 1$ is allowed.

	λ_L	λ_u	λ_d
I	$[-0.22, 0.42]$	–	–
II	$[-0.12, 0.30]$	–	$[-0.92, 0.96]$
III	$[-0.12, 0.26]$	–	$[-0.88, 0.90]$

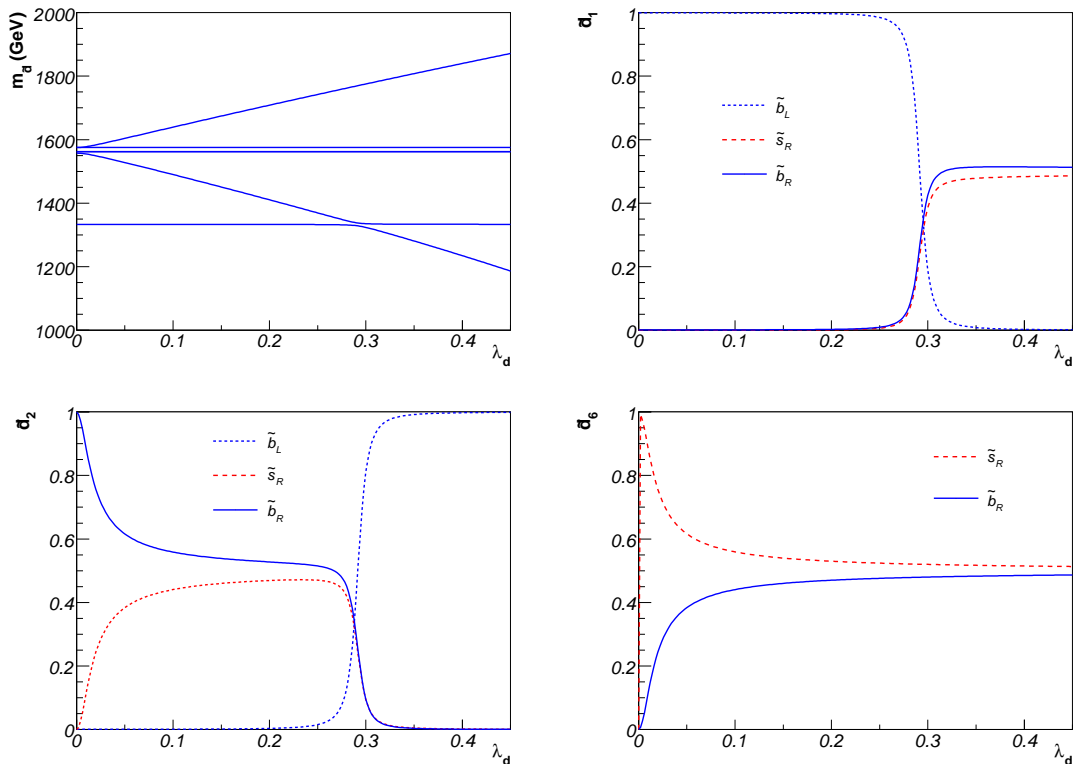


FIG. 5: Dependence of masses and flavour decomposition of the lightest, second lightest, and heaviest down-type squarks on the flavour-violating parameter λ_d for the scenario I of Tab. I.

important. Consequently, the lightest down-type squark \tilde{d}_1 becomes lighter, while the mass of the heaviest down-type state \tilde{d}_6 increases.

The altered mass splitting is accompanied by changes in the flavour decomposition of the involved squark states. In particular, at points where two squark mass eigenvalues should cross, the two corresponding eigenstates exchange their flavour content and undergo a so-called “avoided crossing” [4]. As can be seen in Fig. 5, in the MFV-case the lightest down-type squark \tilde{d}_1 is a pure left-handed sbottom. For $\lambda_d \gtrsim 0.3$, this state acquires a sizeable admixture of the \tilde{s}_R and \tilde{b}_R squark, while its \tilde{b}_L content drops accordingly. In a similar fashion, the next-to-lightest down-type squark \tilde{d}_2 is purely bottom-like at $\lambda_d = 0$ and gets a sizeable strange admixture in the flavour-violating case. At $\lambda_d \sim 0.3$, an avoided crossing of the two mass eigenvalues of \tilde{d}_1 and \tilde{d}_2 is observed and the two states exchange their flavour content. For $\lambda_d > 0.3$, the lightest down-type squark is then a mixture of the \tilde{s}_R and \tilde{b}_R eigenstates, whilst the next-to-lightest one becomes a pure \tilde{b}_L state. Among the other mass eigenstates, only the heaviest down-type squark is fairly affected by λ_d mixings. In the absence of additional flavour violation, *i.e.*, in the $\lambda_d = 0$ case, this state is purely \tilde{d}_R -like (not shown in the corresponding graph for the sake of visibility). However, for $\lambda_d \gtrsim 0$, it immediately undergoes an “avoided crossing” with \tilde{d}_5 and exchanges its flavour content, being then a pure \tilde{s}_R state. With increasing values of the λ_d parameter, this squark gradually gets a larger and larger \tilde{b}_R component, and maximal mixing is reached for $\lambda_d \gtrsim 0.4$.

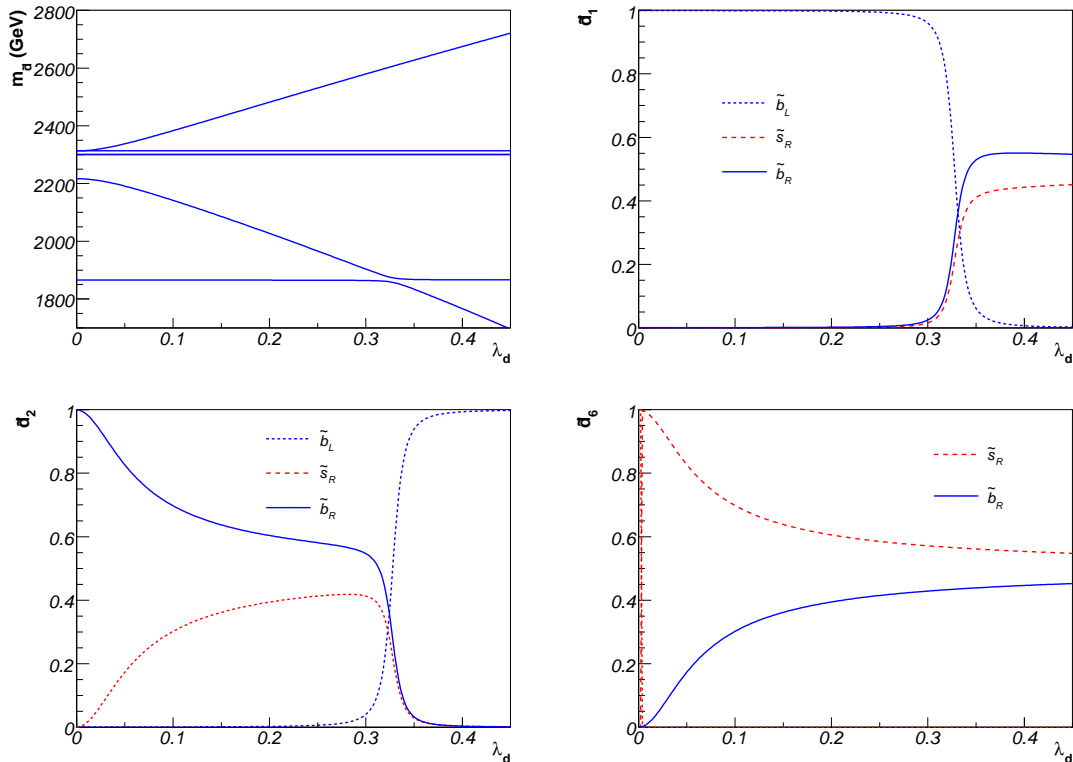


FIG. 6: Same as Fig. 5 for the scenario II of Tab. I.

Avoided crossings and similar mass splittings also occur for the two other scenarios, as presented in Figs. 6 and 7, as well as for up-type squarks and the variations of the other flavour-violating parameters λ_L and λ_u (not shown). This behaviour can lead to interesting phenomenological consequences for production and decays of squarks and gluinos, as it has been shown in Refs. [4, 5, 56–61]. In particular, the dependence of the gluino production on the non-minimal flavour-violation parameters is discussed in the following Section.

In Figs. 8, 9 and 10, we show the theoretical predictions for the branching ratios of the rare decays $b \rightarrow s\gamma$ and $b \rightarrow s\mu\mu$ as well as the meson-oscillation observable $\Delta M_{B_s^0}$ as a function of the left-left mixing parameter λ_L . These three observables are rather sensitive to non-minimal flavour violation and can therefore be used to constrain the possible values of the λ -parameters, contrary to the branching ratio $B_s^0 \rightarrow \mu^+\mu^-$, for which the predictions lie well below the observed upper bound of Eq. (3.4), for any value for the λ -parameters, and are given by $(5.0 \dots 5.2) \times 10^{-9}$, $(5.2 \dots 6.3) \times 10^{-9}$ and $(5.0 \dots 9.0) \times 10^{-9}$ for our scenarios I, II and III, respectively. As already discussed above, the decay $b \rightarrow s\gamma$ is very sensitive to additional flavour mixing, particularly in the left-left sector. Together with its high experimental precision, this makes it the most stringent constraint in this case. Hence, as shown in the figures, the lower limit of the interval given in Eq. (3.2) is reached (at the 2σ confidence level) at $\lambda_L \sim 0.4$, according to the corresponding values derived in Tab. II. The prediction of $\Delta M_{B_s^0}$ also strongly depends on the mixing in the left-left chiral sector. The lower bound of Eq. (3.5) is reached at $\lambda_L \sim 0.43$, making this constraint competitive to the rare decay $b \rightarrow s\gamma$ despite the large theoretical uncertainty. Finally, constraints from the $b \rightarrow s\mu\mu$ observable are weaker for values of the mixing-parameter $\lambda_L \lesssim 0.6$, the theoretical predictions showing no significant dependence on flavour mixing in that λ_L -region.

4. NON-MINIMALLY FLAVOUR VIOLATING GLUINO HADROPRODUCTION

4.1. Generalized couplings in NMFV supersymmetry

In our previous publications, we have computed the cross sections for the production of gaugino and squark pairs in the framework of non-minimally flavour-violating supersymmetry [4, 5]. In this work, we add the missing channels

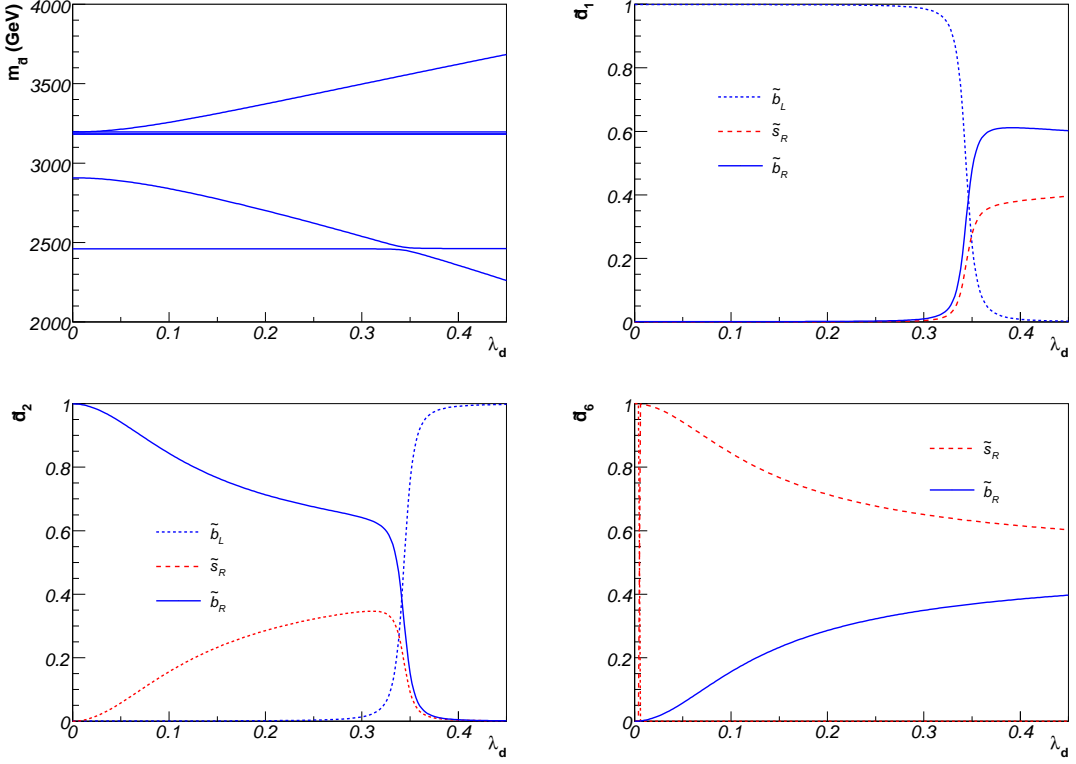


FIG. 7: Same as Fig. 5 for the scenario III of Tab. I.

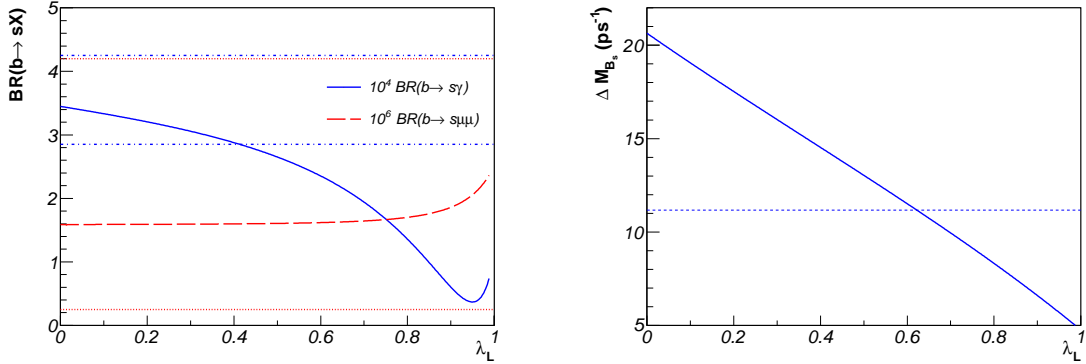


FIG. 8: Dependence of $\text{BR}(b \rightarrow s\gamma)$, $\text{BR}(b \rightarrow s\mu\mu)$, and $\Delta M_{B_s^0}$ on the flavour-violating parameter λ_L for the scenario I of Tab. I. We also show horizontal lines corresponding to the experimental upper and lower limits for $\text{BR}(b \rightarrow s\gamma)$ (blue dashed), $\text{BR}(b \rightarrow s\mu\mu)$ (red dotted), and $\Delta M_{B_s^0}$ (blue dashed), as discussed in Sec. 3.1.

related to gluino production. We first introduce our conventions for the generalized strong and electroweak couplings which will appear in our analytical calculations of the cross sections. Non-minimal flavour violation in the strong sector can arise from interactions between gluinos \tilde{g} , quarks q and left- (right-)handed squarks \tilde{q}_L (\tilde{q}_R) described by the (flavour-diagonal) Lagrangian [1, 2]

$$\mathcal{L}_{q\tilde{q}\tilde{g}} = \sqrt{2}g_s \left[-\tilde{q}_{Lf}^\dagger T_a (\tilde{g}^\alpha P_L \tilde{q}_f) + (\tilde{q}_f P_L \tilde{g}^a) T_a \tilde{q}_{Rf} \right] + \text{h.c.}, \quad (4.1)$$

where f stands for a flavour index, T_a and g_s are the fundamental matrices and the coupling constant associated with the $SU(3)_c$ gauge group, and P_L denotes the left-chirality projection operator acting on four-component spinors.

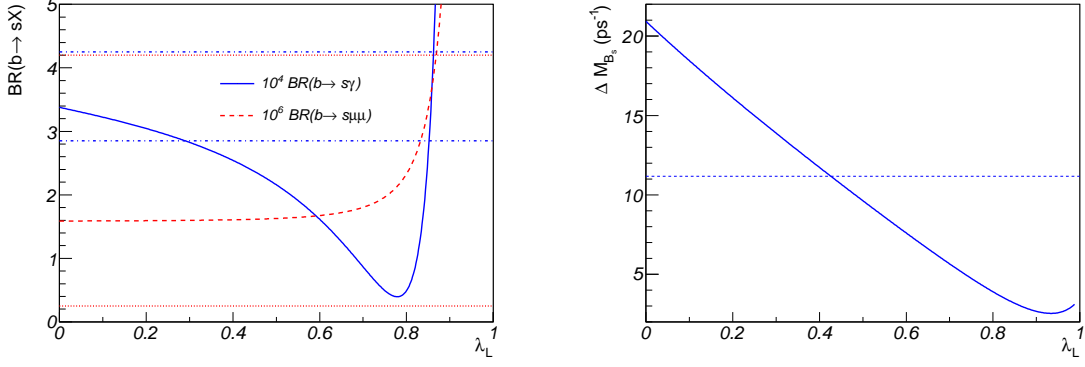


FIG. 9: Same as Fig. 8 for the scenario II of Tab. I.

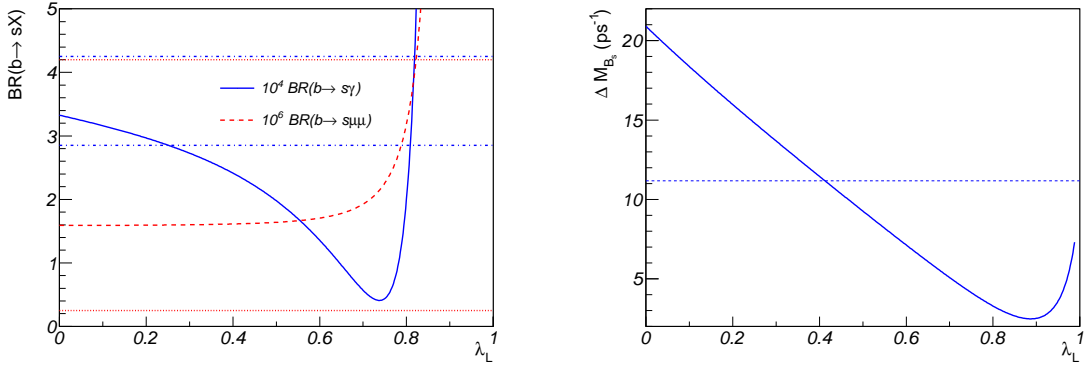


FIG. 10: Same as Fig. 8 for the scenario III of Tab. I.

Rotating to the mass-eigenstate basis, flavour violation is introduced through possible non-diagonal entries in the matrices R^q . In this case, the left-handed and right-handed coupling strengths become proportional to

$$\left\{ L_{\bar{q}_i q_j \bar{g}}, R_{\bar{q}_i q_j \bar{g}} \right\} = \left\{ R_{ij}^q, -R_{i(j+3)}^q \right\}. \quad (4.2)$$

Similarly, for the electroweak sector, non-minimally flavour-violating interactions can arise in the chargino and neutralino couplings to quarks and squarks. We start from the Lagrangian

$$\begin{aligned} \mathcal{L}_{q\bar{q}\tilde{\chi}} = & \sqrt{2}g' \left[-\frac{1}{6} \bar{q}_{L_f}^\dagger (\tilde{B} P_L q_f) + \frac{2}{3} (\bar{u}_f P_L \tilde{B}) \tilde{u}_{R_f} - \frac{1}{3} (\bar{d}_f P_L \tilde{B}) \tilde{d}_{R_f} \right] - \frac{\sqrt{2}}{2} g_W \tilde{Q}_f^\dagger \sigma_k (\tilde{W}^k P_L Q_f) \\ & - (y_d)_{ff'} \bar{d}_f^\dagger \tilde{H}_d P_L Q_{f'} + (y_d)_{ff'} \tilde{Q}_{f'} \bar{d}_f P_L \tilde{H}_d + (y_u)_{ff'} \tilde{u}_f^\dagger \tilde{H}_u P_L Q_{f'} - (y_u)_{ff'} \tilde{Q}_{f'} \bar{u}_f P_L \tilde{H}_u + \text{h.c.}, \end{aligned} \quad (4.3)$$

where \tilde{B} , \tilde{W} and $\tilde{H}_{\{u,d\}}$ are the four-component bino-, wino- and higgsino-eigenstates and Q (\tilde{Q}), u (\tilde{u}) and d (\tilde{d}) the doublet of left-handed (s)quarks and the up- and down-type right-handed (s)quarks, respectively. In the Lagrangian above, we denote the hypercharge and weak coupling constants g' and g_W , while the generators of $SU(2)_L$ are given by $\sigma/2$, σ being the Pauli matrices. Finally, y_u and y_d are the up-type and down-type quark Yukawa matrices, which once diagonalized are proportional to the quark masses,

$$(\hat{y}_u)_{ij} = \frac{\sqrt{2}g_W m_{u_i}}{2m_W \sin \beta} \delta_{ij} \quad \text{and} \quad (\hat{y}_d)_{ij} = \frac{\sqrt{2}g_W m_{d_i}}{2m_W \cos \beta} \delta_{ij}. \quad (4.4)$$

Here, $\hat{y}_{\{u,d\}}$ denote the diagonalized Yukawa matrices. After rotating to the mass-basis, one obtains the coupling strengths

$$\begin{aligned}
L_{\bar{d}_j d_k \bar{\chi}_i^0} &= \frac{(e_d - T_d^3) s_W N_{i1} + T_d^3 c_W N_{i2}}{\sqrt{2} c_W} R_{jk}^{d*} + \frac{m_{d_k} N_{i3}}{2\sqrt{2} m_W \cos \beta} R_{j(k+3)}^{d*} , \\
R_{\bar{d}_j d_k \bar{\chi}_i^0} &= -\frac{e_d s_W N_{i1}^*}{\sqrt{2} c_W} R_{j(k+3)}^{d*} + \frac{m_{d_k} N_{i3}^*}{2\sqrt{2} m_W \cos \beta} R_{jk}^{d*} , \\
L_{\bar{u}_j u_k \bar{\chi}_i^0} &= \frac{(e_u - T_u^3) s_W N_{i1} + T_u^3 c_W N_{i2}}{\sqrt{2} c_W} R_{jk}^{u*} + \frac{m_{u_k} N_{i4}}{2\sqrt{2} m_W \sin \beta} R_{j(k+3)}^{u*} , \\
R_{\bar{u}_j u_k \bar{\chi}_i^0} &= -\frac{e_u s_W N_{i1}^*}{\sqrt{2} c_W} R_{j(k+3)}^{u*} + \frac{m_{u_k} N_{i4}^*}{2\sqrt{2} m_W \sin \beta} R_{jk}^{u*} , \\
L_{\bar{d}_j u_k \bar{\chi}_i^\pm} &= \frac{1}{2} \sum_{l=1}^3 \left[U_{i1} R_{jl}^{d*} - \frac{m_{d_l} U_{i2}}{\sqrt{2} m_W \cos \beta} R_{j(l+3)}^{d*} \right] V_{u_k d_l} , \\
R_{\bar{d}_j u_k \bar{\chi}_i^\pm} &= -\sum_{l=1}^3 \frac{m_{u_k} V_{i2}^* V_{u_k d_l}}{2\sqrt{2} m_W \sin \beta} R_{jl}^{d*} , \\
L_{\bar{u}_j d_k \bar{\chi}_i^\pm} &= \frac{1}{2} \sum_{l=1}^3 \left[V_{i1} R_{jl}^{u*} - \frac{m_{u_l} V_{i2}}{\sqrt{2} m_W \sin \beta} R_{j(l+3)}^{u*} \right] V_{u_l d_k}^* , \\
R_{\bar{u}_j d_k \bar{\chi}_i^\pm} &= -\sum_{l=1}^3 \frac{m_{d_k} U_{i2}^* V_{u_l d_k}^*}{2\sqrt{2} m_W \cos \beta} R_{jl}^{u*} ,
\end{aligned} \tag{4.5}$$

where we follow the notations of Sec. 2. In addition, we introduce the mass of the W -boson m_W , the cosine of the electroweak mixing angle c_W , and the matrices N , U and V related to the gaugino/higgsino mixing.

4.2. Analytical results

We compute the partonic cross sections related to gluino production, *i.e.*, for the processes

$$a_{h_a}(p_a) b_{h_b}(p_b) \rightarrow \tilde{g}(p_1) \tilde{q}_i^{(*)}(p_2) , \quad \tilde{g}(p_1) \tilde{g}(p_2) \quad \text{and} \quad \tilde{g}(p_1) \tilde{\chi}_i^{\{\pm,0\}}(p_2) , \tag{4.6}$$

and present the results for definite helicities $h_{a,b}$ of the initial partons $a, b = q, \bar{q}, g$ in terms of the squark masses $m_{\tilde{q}_j}$, the chargino and neutralino masses $m_{\tilde{\chi}_j}$, the gluino mass $m_{\tilde{g}}$, the Mandelstam variables

$$s = (p_a + p_b)^2 , \quad t = (p_a - p_1)^2 , \quad \text{and} \quad u = (p_a - p_2)^2 , \tag{4.7}$$

and the mass-subtracted Mandelstam variables

$$t_{\tilde{g}} = t - m_{\tilde{g}}^2 , \quad u_{\tilde{g}} = u - m_{\tilde{g}}^2 , \quad t_{\tilde{q}_i} = t - m_{\tilde{q}_i}^2 , \quad u_{\tilde{q}_i} = u - m_{\tilde{q}_i}^2 , \quad t_{\tilde{\chi}_i} = t - m_{\tilde{\chi}_i}^2 , \quad u_{\tilde{\chi}_i} = u - m_{\tilde{\chi}_i}^2 . \tag{4.8}$$

Unpolarized partonic cross sections $d\hat{\sigma}$ and single- and double-polarized cross partonic sections $d\hat{\sigma}_L$ and $d\hat{\sigma}_{LL}$, averaged over initial spins, can easily be derived from the helicity-dependent result,

$$\begin{aligned}
d\hat{\sigma} &= \frac{d\hat{\sigma}_{1,1} + d\hat{\sigma}_{1,-1} + d\hat{\sigma}_{-1,1} + d\hat{\sigma}_{-1,-1}}{4} , \\
d\Delta\hat{\sigma}_L &= \frac{d\hat{\sigma}_{1,1} + d\hat{\sigma}_{1,-1} - d\hat{\sigma}_{-1,1} - d\hat{\sigma}_{-1,-1}}{4} , \\
d\Delta\hat{\sigma}_{LL} &= \frac{d\hat{\sigma}_{1,1} - d\hat{\sigma}_{1,-1} - d\hat{\sigma}_{-1,1} + d\hat{\sigma}_{-1,-1}}{4} .
\end{aligned} \tag{4.9}$$

The strong production of a pair of gluinos proceeds either from the annihilation of a quark-antiquark pair in the initial state,

$$q_{h_a}(p_a) \bar{q}_{h_b}(p_b) \rightarrow \tilde{g}(p_1) \tilde{g}(p_2) , \tag{4.10}$$

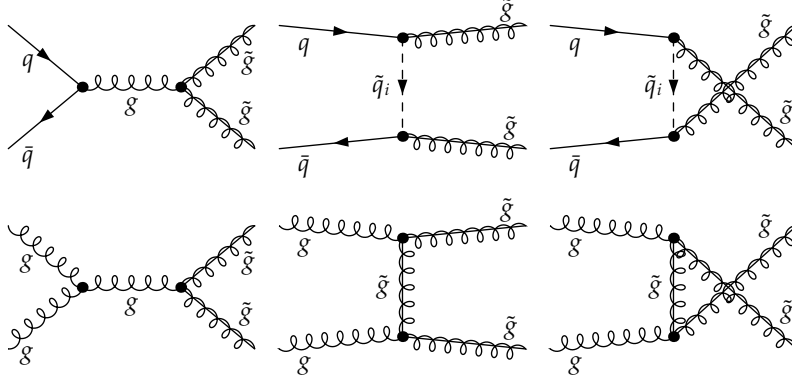


FIG. 11: Tree-level Feynman diagrams for the production of a pair of gluinos in quark-antiquark (top) and gluon-gluon collisions (bottom).

as shown in Fig. 11 (top), or from the fusion of two initial gluons,

$$g_{h_a}(p_a) g_{h_b}(p_b) \rightarrow \tilde{g}(p_1) \tilde{g}(p_2), \quad (4.11)$$

as can be seen in the lower part of Fig. 11. Since the latter is independent of squark exchange, the corresponding differential partonic cross section, averaged on the initial colour states and taking into account the symmetry factor relative to the production of two identical particles, is independent from any possible source of flavour violation in the squark sector. It is given by

$$\frac{d\hat{\sigma}}{dt}(h_a, h_b) = \frac{g_s^4 N_c^2}{16\pi s^2 (N_c^2 - 1)} \left(1 - \frac{t_{\tilde{g}} u_{\tilde{g}}}{s^2} \right) \left[(1 - h_a h_b) \left(-2 + \frac{s^2}{t_{\tilde{g}} u_{\tilde{g}}} + 4 \frac{sm_{\tilde{g}}^2}{t_{\tilde{g}} u_{\tilde{g}}} \left[1 - \frac{sm_{\tilde{g}}^2}{t_{\tilde{g}} u_{\tilde{g}}} \right] \right) + 2h_a h_b (s - 2m_{\tilde{g}}^2) \frac{m_{\tilde{g}}^2 s^2}{t_{\tilde{g}}^2 u_{\tilde{g}}^2} \right], \quad (4.12)$$

where N_c denotes the number of colours. This result agrees with those of Refs. [62, 63] after summing over the initial gluon polarizations. Contrary, the quark-antiquark channel contains t -channel and u -channel squark exchanges. However, even if a given squared diagram or interference term depended on some combination of the element of the squark mixing matrices, the sum over all possible squark exchanges is expected to considerably reduce the flavour-violation dependence of the cross section. The latter can be expressed as

$$\begin{aligned} \frac{d\hat{\sigma}}{dt}(h_a, h_b) = & \frac{g_s^4}{128\pi s^2 N_c^2} \left[(1 - h_a)(1 + h_b) \left[\frac{Q_{ss}}{s^2} + \sum_{i=1}^6 \left\{ \frac{(Q_{st})_i^1}{st_{\tilde{q}_i}} + \frac{(Q_{su})_i^1}{su_{\tilde{q}_i}} \right\} + \sum_{i,j=1}^6 \left\{ \frac{(Q_{tt})_{ij}^{11}}{t_{\tilde{q}_i} t_{\tilde{q}_j}} + \frac{(Q_{uu})_{ij}^{11}}{u_{\tilde{q}_i} u_{\tilde{q}_j}} + \frac{(Q_{tu})_{ij}^{11}}{t_{\tilde{q}_i} u_{\tilde{q}_j}} \right\} \right] \right. \\ & + (1 + h_a)(1 - h_b) \left[\frac{Q_{ss}}{s^2} + \sum_{i=1}^6 \left\{ \frac{(Q_{st})_i^2}{st_{\tilde{q}_i}} + \frac{(Q_{su})_i^2}{su_{\tilde{q}_i}} \right\} + \sum_{i,j=1}^6 \left\{ \frac{(Q_{tt})_{ij}^{22}}{t_{\tilde{q}_i} t_{\tilde{q}_j}} + \frac{(Q_{uu})_{ij}^{22}}{u_{\tilde{q}_i} u_{\tilde{q}_j}} + \frac{(Q_{tu})_{ij}^{22}}{t_{\tilde{q}_i} u_{\tilde{q}_j}} \right\} \right] \\ & + (1 - h_a)(1 - h_b) \left[\sum_{i,j=1}^6 \left\{ \frac{(Q_{tt})_{ij}^{12}}{t_{\tilde{q}_i} t_{\tilde{q}_j}} + \frac{(Q_{uu})_{ij}^{12}}{u_{\tilde{q}_i} u_{\tilde{q}_j}} + \frac{(Q_{tu})_{ij}^{12}}{t_{\tilde{q}_i} u_{\tilde{q}_j}} \right\} \right] \\ & \left. + (1 + h_a)(1 + h_b) \left[\sum_{i,j=1}^6 \left\{ \frac{(Q_{tt})_{ij}^{21}}{t_{\tilde{q}_i} t_{\tilde{q}_j}} + \frac{(Q_{uu})_{ij}^{21}}{u_{\tilde{q}_i} u_{\tilde{q}_j}} + \frac{(Q_{tu})_{ij}^{21}}{t_{\tilde{q}_i} u_{\tilde{q}_j}} \right\} \right] \right] \quad (4.13) \end{aligned}$$

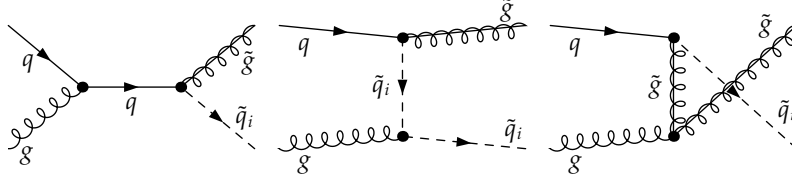


FIG. 12: Tree-level Feynman diagrams for the associated production of gluinos and squarks.

with the generalized charges

$$\begin{aligned}
Q_{ss} &= 2N_c(N_c^2 - 1) \left(t_{\tilde{g}}^2 + u_{\tilde{g}}^2 + 2m_{\tilde{g}}^2 s \right), \\
(Q_{st})_i^m &= N_c(N_c^2 - 1) \operatorname{Re} \left[C_{\tilde{q}_i q \tilde{g}}^m C_{\tilde{q}_i q' \tilde{g}}^{m*} \right] \left(m_{\tilde{g}}^2 s + t_{\tilde{g}}^2 \right), \\
(Q_{su})_i^m &= N_c(N_c^2 - 1) \operatorname{Re} \left[C_{\tilde{q}_i q \tilde{g}}^m C_{\tilde{q}_i q' \tilde{g}}^{m*} \right] \left(m_{\tilde{g}}^2 s + u_{\tilde{g}}^2 \right), \\
(Q_{tt})_{ij}^{mn} &= \frac{(N_c^2 - 1)^2}{N_c} C_{\tilde{q}_i q \tilde{g}}^m C_{\tilde{q}_i q' \tilde{g}}^{n*} C_{\tilde{q}_j q \tilde{g}}^{m*} C_{\tilde{q}_j q' \tilde{g}}^n t_{\tilde{g}}^2, \\
(Q_{uu})_{ij}^{mn} &= \frac{(N_c^2 - 1)^2}{N_c} C_{\tilde{q}_i q \tilde{g}}^m C_{\tilde{q}_i q' \tilde{g}}^{n*} C_{\tilde{q}_j q \tilde{g}}^{m*} C_{\tilde{q}_j q' \tilde{g}}^n u_{\tilde{g}}^2, \\
(Q_{tu})_{ij}^{mn} &= 2 \frac{(N_c^2 - 1)}{N_c} \operatorname{Re} \left[C_{\tilde{q}_i q \tilde{g}}^m C_{\tilde{q}_i q' \tilde{g}}^{n*} C_{\tilde{q}_j q' \tilde{g}}^n C_{\tilde{q}_j q \tilde{g}}^{m*} \right] \left((1 - \delta_{mn})(m_{\tilde{g}}^2 s - t_{\tilde{g}} u_{\tilde{g}}) + \delta_{mn} m_{\tilde{g}}^2 s \right),
\end{aligned} \tag{4.14}$$

where for the sake of simplicity we have introduced the generic notation

$$\{ \mathcal{C}_{abc}^1, \mathcal{C}_{abc}^2 \} = \{ L_{abc}, R_{abc} \}. \tag{4.15}$$

This reproduces both the polarized and unpolarized results of Refs. [62, 63] in the flavour-conserving MSSM limit.

An associated pair of a gluino and a squark originates from quark-gluon initial states,

$$q_{h_a}(p_a) g_{h_b}(p_b) \rightarrow \tilde{g}(p_1) \tilde{q}_i(p_2), \tag{4.16}$$

and proceeds through an s -channel quark, t -channel squark, or u -channel gluino exchange as it is illustrated in Fig. 12. Since each contribution involves a coupling between a quark, a squark and a gluino, this process can in general violate flavour. The differential cross section is given by

$$\begin{aligned}
\frac{d\hat{\sigma}}{dt}(h_a, h_b) &= \frac{g_s^4}{64\pi s^2} \left\{ \left[(1-h_a)(1-h_b) |L_{\tilde{q}_i q \tilde{g}}|^2 + (1+h_a)(1+h_b) |R_{\tilde{q}_i q \tilde{g}}|^2 \right] \right. \\
&\quad \times \left[\frac{-(N_c^2 - 1)u_{\tilde{g}}}{4N_c^2 s} + \frac{st + t_{\tilde{g}} t_{\tilde{q}_i}}{2N_c^2 st_{\tilde{q}_i}} + \frac{1}{2u_{\tilde{g}}} \left(\frac{2su - su_{\tilde{g}} + 2u_{\tilde{q}_i} u_{\tilde{g}}}{u_{\tilde{g}}} + \frac{m_{\tilde{g}}^2 s + u_{\tilde{g}} u_{\tilde{q}_i}}{s} + \frac{m_{\tilde{g}}^2 m_{\tilde{q}_i}^2 - tu}{t_{\tilde{q}_i}} \right) \right] \\
&\quad + \left[(1-h_a) |L_{\tilde{q}_i q \tilde{g}}|^2 + (1+h_a) |R_{\tilde{q}_i q \tilde{g}}|^2 \right] \\
&\quad \times \left. \left[\frac{(N_c^2 - 1)m_{\tilde{q}_i}^2 t_{\tilde{g}}}{2N_c^2 t_{\tilde{q}_i}^2} - \frac{t_{\tilde{g}}(s + t_{\tilde{g}})}{2N_c^2 st_{\tilde{q}_i}} \frac{1}{2u_{\tilde{g}}} \left(\frac{2ut_{\tilde{g}}}{u_{\tilde{g}}} - \frac{u_{\tilde{q}_i}(s + u_{\tilde{q}_i})}{s} + \frac{2u - u_{\tilde{q}_i}}{t_{\tilde{q}_i}} \right) \right] \right\},
\end{aligned} \tag{4.17}$$

which agrees again with the polarized and unpolarized results of Refs. [62, 63] in the flavour-conserving MSSM limit and after summing over mass-degenerate squarks. The cross section for the charge-conjugate process can be easily derived by replacing $h_a \rightarrow -h_a$.

Finally, the associated production of a gluino and a chargino or of a gluino and a neutralino,

$$q_{h_a}(p_a) \bar{q}_{h_b}(p_b) \rightarrow \tilde{g}(p_1) \tilde{\chi}_i^{\pm,0}(p_2), \tag{4.18}$$

can be mediated through a t -channel or u -channel squark exchange, as shown in Fig. 13, and can thus involve flavour-

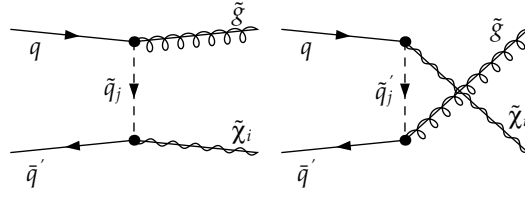


FIG. 13: Tree-level Feynman diagrams for the associated production of gluinos and gauginos.

violating interactions. The differential cross section is given by

$$\begin{aligned}
\frac{d\hat{\sigma}}{dt}(h_a, h_b) &= \frac{g_s^2 g_W^2 (N_c^2 - 1)}{8\pi s^2 N_c^2} \sum_{i,j=1}^6 \left\{ (1-h_a)(1+h_b) \left[\frac{(Q_{tt})_{ij}^{11}}{t_{\tilde{q}_i} t_{\tilde{q}_j}} + \frac{(Q_{uu})_{ij}^{11}}{u_{\tilde{q}_i} u_{\tilde{q}_j}} + \frac{(Q_{tu})_{ij}^{11}}{t_{\tilde{q}_i} u_{\tilde{q}_j}} \right] \right. \\
&+ (1+h_a)(1-h_b) \left[\frac{(Q_{tt})_{ij}^{22}}{t_{\tilde{q}_i} t_{\tilde{q}_j}} + \frac{(Q_{uu})_{ij}^{22}}{u_{\tilde{q}_i} u_{\tilde{q}_j}} + \frac{(Q_{tu})_{ij}^{22}}{t_{\tilde{q}_i} u_{\tilde{q}_j}} \right] \\
&+ (1-h_a)(1-h_b) \left[\frac{(Q_{tt})_{ij}^{12}}{t_{\tilde{q}_i} t_{\tilde{q}_j}} + \frac{(Q_{uu})_{ij}^{12}}{u_{\tilde{q}_i} u_{\tilde{q}_j}} + \frac{(Q_{tu})_{ij}^{12}}{t_{\tilde{q}_i} u_{\tilde{q}_j}} \right] \\
&\left. + (1+h_a)(1+h_b) \left[\frac{(Q_{tt})_{ij}^{21}}{t_{\tilde{q}_i} t_{\tilde{q}_j}} + \frac{(Q_{uu})_{ij}^{21}}{u_{\tilde{q}_i} u_{\tilde{q}_j}} + \frac{(Q_{tu})_{ij}^{21}}{t_{\tilde{q}_i} u_{\tilde{q}_j}} \right] \right\}, \tag{4.19}
\end{aligned}$$

where we have introduced the generalized charges,

$$\begin{aligned}
(Q_{tt})_{ij}^{mn} &= C_{\tilde{q}_i q \tilde{g}}^{m*} C_{\tilde{q}_i q' \tilde{\chi}_i}^{n*} C_{\tilde{q}_j q \tilde{g}}^m C_{\tilde{q}_j q' \tilde{\chi}_i}^n t_{\tilde{g}}^2 t_{\tilde{\chi}_i}, \\
(Q_{uu})_{ij}^{mn} &= C_{\tilde{q}_i q' \tilde{g}}^{m*} C_{\tilde{q}_i q \tilde{\chi}_i}^{n*} C_{\tilde{q}_j q' \tilde{g}}^m C_{\tilde{q}_j q \tilde{\chi}_i}^n u_{\tilde{g}}^2 u_{\tilde{\chi}_i}, \\
(Q_{tu})_{ij}^{mn} &= 2\text{Re} \left[C_{\tilde{q}_i q \tilde{g}}^{m*} C_{\tilde{q}_i q' \tilde{\chi}_i}^{n*} C_{\tilde{q}_j q' \tilde{g}}^m C_{\tilde{q}_j q \tilde{\chi}_i}^n u_{\tilde{g}}^2 u_{\tilde{\chi}_i} \right] \left((1 - \delta_{mn})(ut - m_{\tilde{g}}^2 m_{\tilde{\chi}_i}^2) - \delta_{mn} m_{\tilde{g}} m_{\tilde{\chi}_i} s \right). \tag{4.20}
\end{aligned}$$

4.3. Numerical predictions for NMFV gluino production at the LHC

In this section, we present numerical predictions in the context of non-minimally flavour violating supersymmetry at the LHC for cross sections related to the production of gluino pairs as well as to the one of associated pairs of a gluino and a squark, an antisquark, a chargino or a neutralino. Squarks and gluinos are expected to be copiously produced at the LHC, due to their strong couplings to quarks and gluons. However, in the case of the benchmark scenarios presented in Tab. I, the high mass of the coloured superpartners drastically reduces the LHC sensitivity, most of the channels being hence largely phase-space suppressed. Therefore, we focus on pp -collisions at the LHC design centre-of-mass energy of $\sqrt{S} = 14$ TeV, supposed to be reached in the second phase of the running of the LHC, after the shutdown of 2013.

Thanks to the QCD factorization theorem, total hadronic production cross sections can be computed by convolving the partonic cross sections derived in Sec. 4.2, summed and averaged over final and initial spins, respectively, with the universal parton densities $f_{a/p}$ and $f_{b/p}$ of partons a, b in the proton, which depend on the longitudinal momentum fractions of the two partons $x_{a,b} = \sqrt{\tau} e^{\pm y}$ and on the unphysical factorization scale μ_F ,

$$\sigma = \int_{4m^2/S}^1 d\tau \int_{-1/2 \ln \tau}^{1/2 \ln \tau} dy \int_{t_{\min}}^{t_{\max}} dt f_{a/p}(x_a, \mu_F) f_{b/p}(x_b, \mu_F) \frac{d\hat{\sigma}}{dt}. \tag{4.21}$$

Neglecting all quark masses but the top mass, we employ the leading order (LO) set of the CTEQ6 parton density fit [64], which includes $n_f = 5$ light quark flavours and the gluon, but no top-quark density. Consistently, the strong coupling constant g_s is evaluated with the corresponding LO value of the QCD scale $\Lambda_{\text{LO}}^{n_f=5} = 165$ MeV. For all our results, we identify the renormalization scale μ_R with the factorization scale μ_F and set the scales to the average mass of the final state supersymmetric particles m .

For gluino pair production as well as for the associated production of a chargino or a neutralino with a gluino, only the t - and u -channel diagrams depend on the flavour-violating parameters in the squark sector since they contain a squark propagator (see the Feynman diagrams shown in Figs. 11 and 13). However, all squark eigenstates contribute

TABLE III: Cross sections, in fb, for the production of pairs of gluinos ($pp \rightarrow \tilde{g}\tilde{g}$), for the one of associated pairs of gluinos and charginos ($pp \rightarrow \tilde{g}\tilde{\chi}_i^+ + \tilde{g}\tilde{\chi}_i^-$ for $i = 1, 2$) and for the one of associated pairs of gluinos and neutralinos ($pp \rightarrow \tilde{g}\tilde{\chi}_i^0$ for $i = 1, 2, 3, 4$), for the reference scenarios presented in Tab. I.

	$\tilde{g}\tilde{g}$	$\tilde{g}\tilde{\chi}_1^\pm$	$\tilde{g}\tilde{\chi}_2^\pm$	$\tilde{g}\tilde{\chi}_1^0$	$\tilde{g}\tilde{\chi}_2^0$	$\tilde{g}\tilde{\chi}_3^0$	$\tilde{g}\tilde{\chi}_4^0$
SPS9	93.8	43.8	0.055	5.1	0.46	0.006	0.001
I	76.5	29.0	0.040	3.3	0.38	0.004	0.001
II	58.9	10.8	0.022	1.2	0.19	0.002	0.001
III	52.5	4.2	0.014	0.47	0.085	0.001	0.001

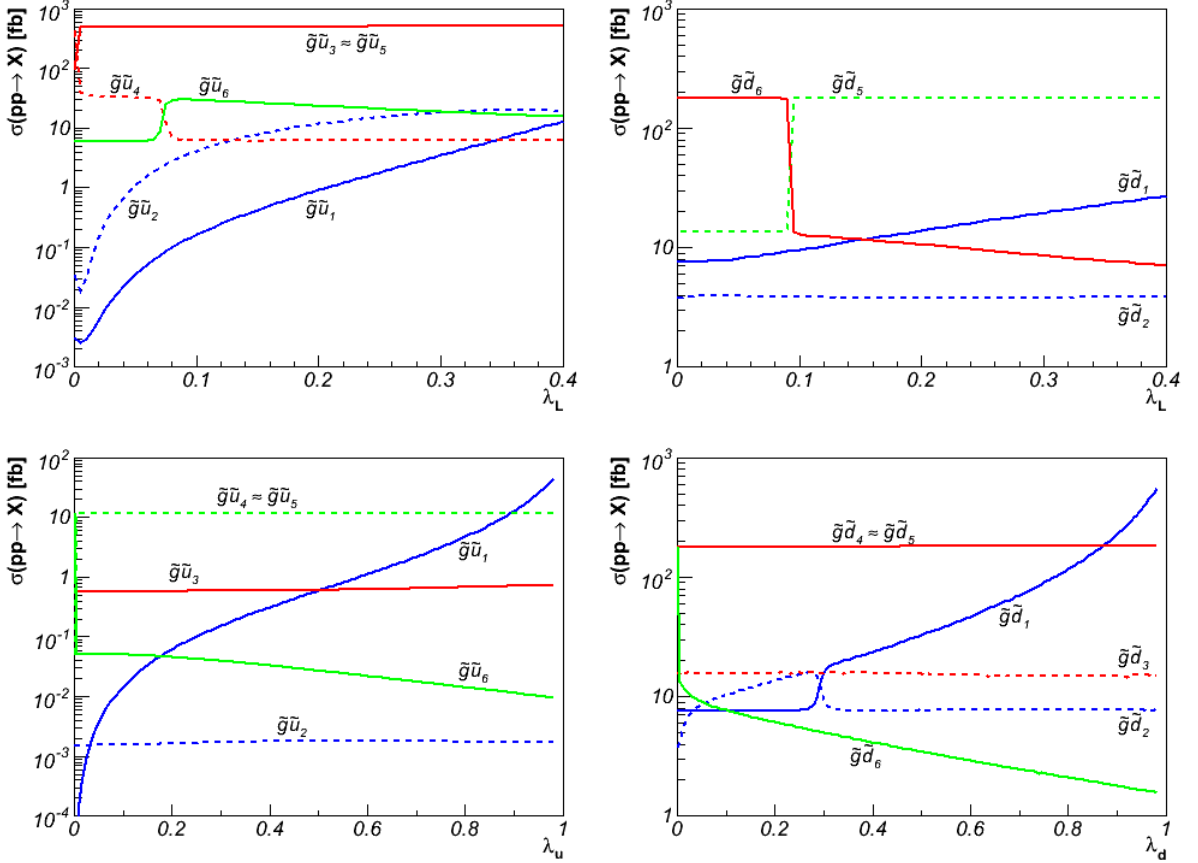


FIG. 14: Cross-sections of gluino production in association with up- and down-type squarks for various ranges of the flavour-mixing parameters λ_L , λ_u , and λ_d for the reference scenario I of Tab. I.

to the total cross section and the corresponding diagrams must be summed over, leading subsequently to production cross sections insensitive to non-minimal flavour-violation. We present these results, therefore independent of the λ -parameters, in Tab. III, both for our scenarios I, II and III as well as for the SPS 9 benchmark point as a reference. Strong gluino pair production is clearly dominant, and the luminosity required to observe possible signal events is not so high. In contrast, the cross sections related to the semi-weak production of a gluino and a chargino/neutralino vary from $\mathcal{O}(10)$ fb for the lightest chargino and neutralino case to the barely visible level of $\mathcal{O}(10^{-3})$ fb for the heavier superpartners.

Contrary to the previous cases, associated squark and gluino production shows an interesting dependence on the non-minimal flavour-violation λ -parameters, as illustrated in Figs. 14, 15 and 16 for our scenarios I, II and III, respectively. Moreover, the cross sections are fairly high, reaching the level of several hundreds of fb for many channels, which makes them nice candidates to study non-minimal flavour violation in supersymmetry at the LHC. Analyzing the dependence of the cross section on the λ -parameters, sharp and smooth transitions can be observed, the first ones being related to the presence of an avoided crossing and the second ones to a smooth change in the

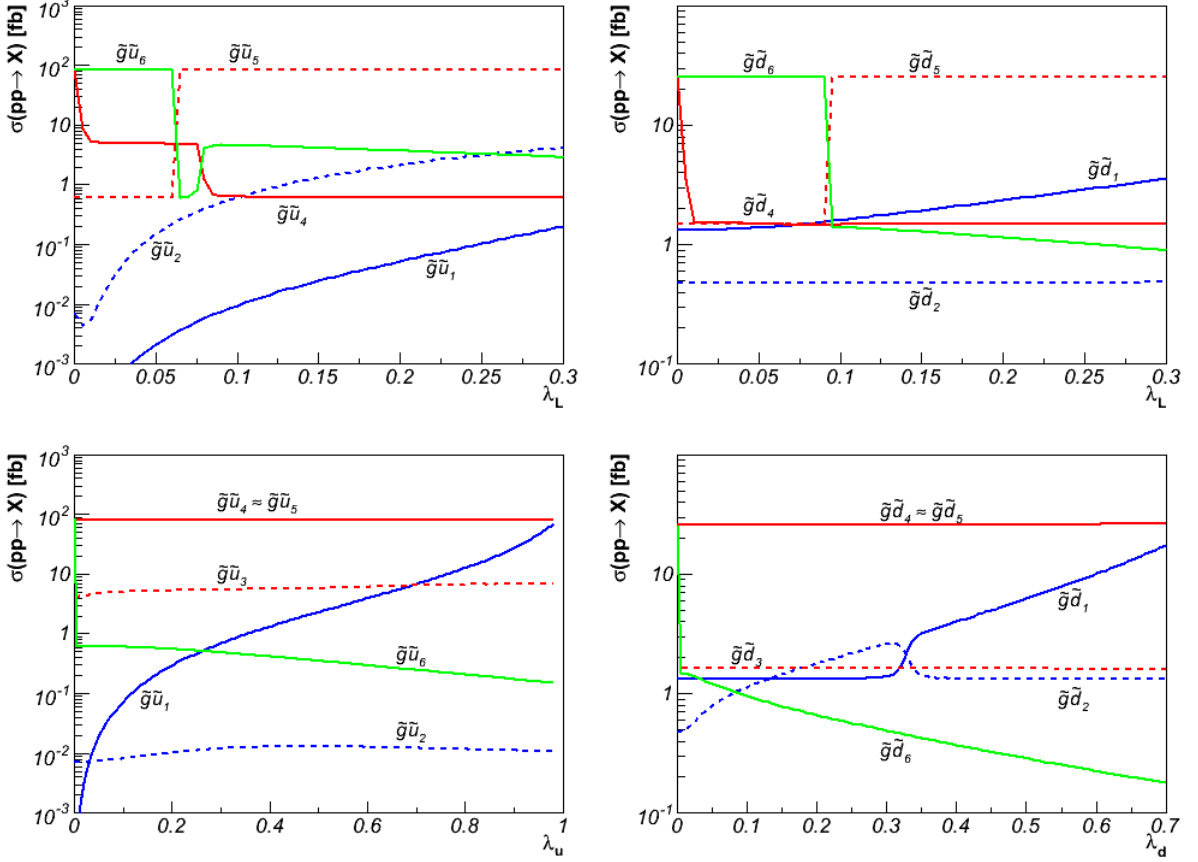


FIG. 15: Same as Fig. 14 for reference scenario II.

flavour content of the relevant eigenstate (see Section 3.3). Indeed, at the point where the mass of two eigenstates should cross, *e.g.*, at $\lambda_L \sim 0.07$ on the top-left panel of Fig. 14 or at $\lambda_d \sim 0.32$ on the lower-right panel of Fig. 15, the flavour content of both squarks is exchanged and the same sharp transition is observed at the level of the cross section. Smooth increases and decreases in the cross section with the values of the λ -parameters have two sources. First, second and third generation squark mixing induces larger mass splitting, as illustrated in Figs. 5, 6 and 7. This renders certain channels phase-space favoured and other channels phase-space suppressed. Secondly, the magnitude of the cross section is connected to the flavour content of the squark produced in association with the gluino, since producing a given flavour of squark requires an initial quark of the same flavour, as shown in the Feynman diagrams of Fig. 12. As an example, the lightest down-type squark mass eigenstate is a pure sbottom state for small values of $\lambda_d \lesssim 0.3$, whilst it becomes a mixed state for $\lambda_d \gtrsim 0.3$, with a larger and larger strange squark component with increasing values of λ_d , as it can be seen from the upper-right panel of Fig. 5. Consequently, as presented in lower-right panel of Fig. 14, the cross section related to the process $pp \rightarrow \tilde{g}\tilde{d}_1$ is small and constant for $\lambda_d \lesssim 0.3$ ($\sigma \approx 8$ fb) and gets larger and larger for increasing λ_d , even reaching a couple of hundreds of fb for $\lambda_d \gtrsim 0.8$. The opposite effects can be observed for the process $pp \rightarrow \tilde{g}\tilde{u}_6$ in the context of the scenario III, as shown in the lower-left panel of Fig. 16.

5. COSMOLOGICAL ASPECTS

Among the most compelling evidences for physics beyond the Standard Model is the presence of cold dark matter (CDM) in our Universe. Its relic density is today constrained to be

$$\Omega_{\text{CDM}} h^2 = 0.1123 \pm 0.0035 \quad (5.1)$$

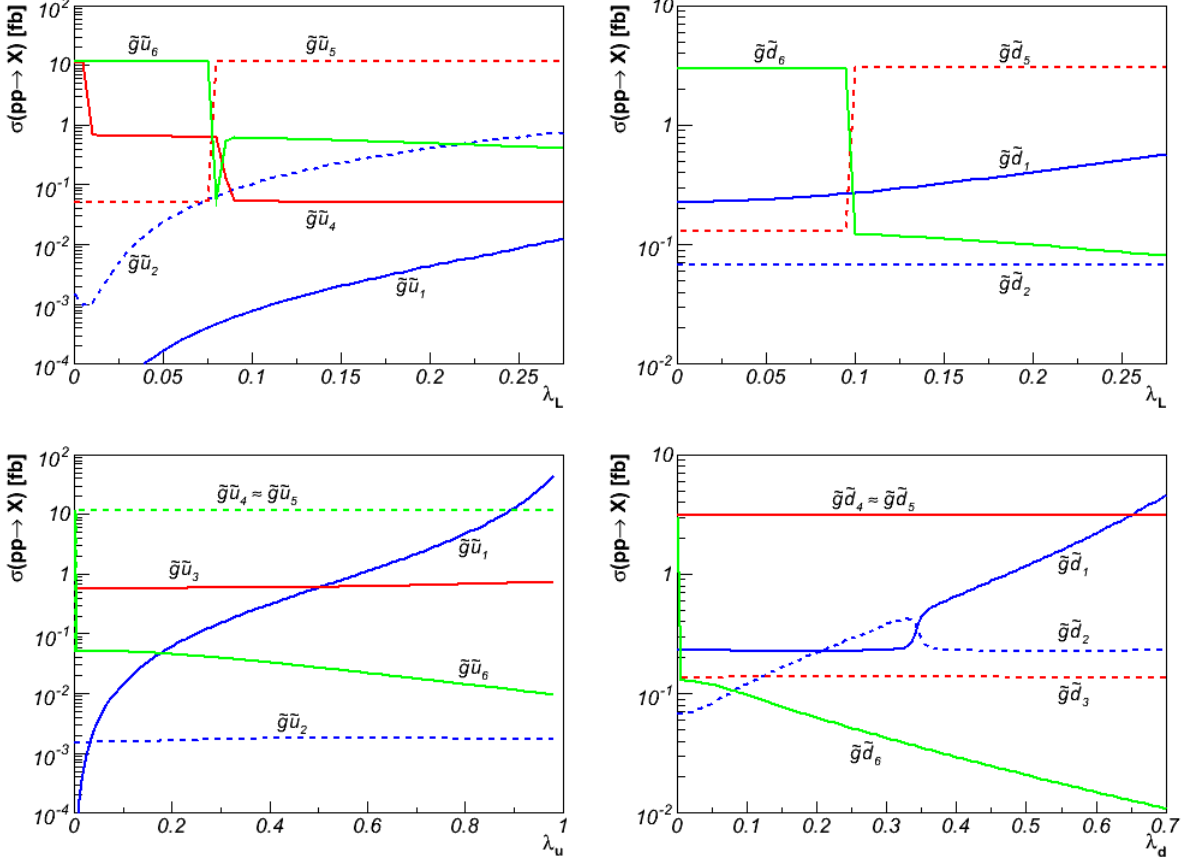


FIG. 16: Same as Fig. 14 for reference scenario III.

from recent WMAP data combined with measurements related to supernovæ and baryonic acoustic oscillations [65]. Here, h is the present Hubble expansion rate in units of $100 \text{ km s}^{-1} \text{ Mpc}^{-1}$. New physics models should therefore include a viable dark matter candidate that can account for the above amount of dark matter.

In AMSB models, the lightest of the four neutralinos is the lightest superpartner and therefore the dark matter candidate, if R-parity is assumed to be conserved. After the renormalization group evolution from the high-scale parameters to the weak scale, the wino mass parameter M_2 turns out to be smaller than the bino and gluino masses M_1 and M_3 . In consequence, in AMSB scenarios the lightest neutralino is wino-like. This is in contrast to, e.g., models based on minimal supergravity where usually $M_1 < M_2$ leading to a bino-like LSP. Since also the chargino mass is governed by M_2 , the mass difference between the lightest neutralino and the lightest chargino is rather small. For our reference scenarios, the mass difference is less than a GeV, as can be seen in Tab. I. Due to the larger pair annihilation cross section as compared to the bino and due to efficient co-annihilations with the chargino, the resulting relic density of the thermally produced neutralino is usually one or two orders of magnitude below the range given in Eq. (5.1) [66, 67]. Using the public programme `DarkSUSY` [68], we obtain the values $\Omega_{\tilde{\chi}_1^0} h^2 = 8.57 \cdot 10^{-4}$, $7.87 \cdot 10^{-4}$, $7.83 \cdot 10^{-4}$, and $7.83 \cdot 10^{-4}$ for the scenarios of Tab. I, respectively.

However, thermal production of neutralinos is not the only mechanism to be considered. Possible non-thermal production modes include the decay of heavy fields such as moduli or gravitinos in the early universe [67, 69]. Moreover, axions and axinos can contribute to the dark matter relic abundance [70, 71]. The contribution to the neutralino relic density from moduli decay can be estimated as [72]

$$\Omega_{\tilde{\chi}_1^0} h^2 \simeq 0.1 \left(\frac{m_{\tilde{\chi}_1^0}}{100 \text{ GeV}} \right) \left(\frac{10.75}{g_*} \right)^{1/4} \left(\frac{3 \cdot 10^{-24} \text{ cm}^3/\text{s}}{\langle \sigma v \rangle} \right) \left(\frac{100 \text{ TeV}}{m_\Phi} \right)^{3/2}. \quad (5.2)$$

It depends on the neutralino mass $m_{\tilde{\chi}_1^0}$, the mass of the moduli fields m_Φ , the effective number of degrees of freedom g_* , and the thermally averaged annihilation cross-section $\langle \sigma v \rangle$. In Fig. 17, we depict isolines of the neutralino relic

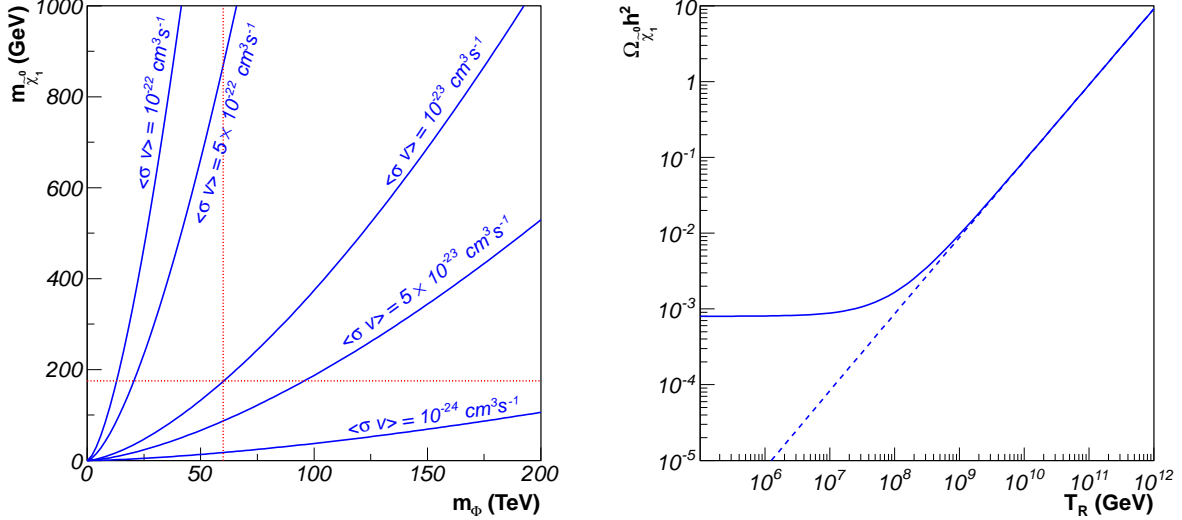


FIG. 17: Left: Isolines corresponding to $\Omega_{\tilde{\chi}_1^0} h^2 = 0.1123$ in the m_Φ - $m_{\tilde{\chi}_1^0}$ planes for different values of $\langle\sigma v\rangle$. The dotted lines correspond to $m_{\tilde{\chi}_1^0} = 175$ GeV and $m_\Phi = m_{3/2} = 60$ TeV. Right: The neutralino relic density $\Omega_{\tilde{\chi}_1^0} h^2$ from gravitino decay as a function of the reheating temperature T_R for a typical AMSB scenarios with $m_{\tilde{\chi}_1^0} = 175$ GeV, $m_{3/2} = 60$ TeV, as it is the case for the scenarios of Tab. I. The solid line includes a contribution of $\Omega_{\tilde{\chi}} h^2 = 8 \cdot 10^{-4}$ from thermal neutralinos, while the dashed line indicates the contribution from gravitino decay only.

density in the $m_{\tilde{\chi}_1^0}$ - m_Φ plane, assuming $g_* \sim 10.75$ [67] and different values of the annihilation cross-section $\langle\sigma v\rangle$. Our typical scenarios lead to a neutralino relic density of about $\Omega_{\tilde{\chi}_1^0} h^2 = 8 \cdot 10^{-4}$, which is consistent with a neutralino annihilation cross-section of $\langle\sigma v\rangle \sim 10^{-23} \text{ cm}^3 \text{ s}^{-1}$. For such cross-sections, a neutralino mass of $m_{\tilde{\chi}_1^0} \sim 175$ GeV and moduli masses comparable with the gravitino mass, $m_\Phi \sim m_{3/2} \sim 60$ TeV, which is consistent with gravity and anomaly mediation [72], this yields nearly the measured abundance of Eq. (5.1).

The neutralino relic abundance from gravitino decay is directly related to the thermal abundance $\Omega_{3/2} h^2$, that the gravitino would have if it did not decay. The latter is obtained from computing the thermal production of gravitinos in the early universe. More precisely, the resulting neutralino relic density can then be evaluated according to [73]

$$\Omega_{\tilde{\chi}_1^0} h^2 = \frac{m_{\tilde{\chi}_1^0}}{m_{3/2}} \Omega_{3/2} h^2 \simeq \frac{m_{\tilde{\chi}_1^0}}{m_{3/2}} \left(\frac{m_{3/2}}{100 \text{ GeV}} \right) \left(\frac{T_R}{10^{10} \text{ GeV}} \right) \sum_{i=1}^3 \omega_i g_i^2 \left(1 + \frac{M_i^2}{3m_{3/2}^2} \right) \log \frac{k_i}{g_i}, \quad (5.3)$$

where the ratio of neutralino and gravitino mass expresses the fact that each gravitino decays into one stable neutralino. The thermal gravitino production depends linearly on the gravitino mass $m_{3/2}$ and the reheating temperature T_R of the universe after inflation. The sum runs over the three gauge groups $U(1)$, $SU(2)$, and $SU(3)$, g_i are the coupling constants of the three gauge groups, and M_i the mass parameters of the associated gauginos. Note that in Eq. (5.3), g_i and M_i are evaluated at the reheating scale T_R . The constants ω_i and k_i are given by $\omega_i = 0.018, 0.044, 0.117$ and $k_i = 1.266, 1.312, 1.271$ for $i = 1, 2, 3$, respectively [73].

The right panel of Fig. 17 shows the resulting neutralino relic density as a function of the reheating temperature for the situation corresponding to the scenarios of Tab. I. For low values of T_R , the thermal neutralino production dominates, leading to the value of $\Omega_{\tilde{\chi}_1^0} h^2 = 8.57 \cdot 10^{-4}$ already mentioned above. For $T_R \gtrsim 10^7$ GeV, the contribution from gravitino decay becomes dominant and $\Omega_{\tilde{\chi}_1^0} h^2$ grows linearly with T_R . As can be seen, the observed relic density of $\Omega_{\tilde{\chi}_1^0} h^2 \sim 0.11$ is obtained for a reheating temperature of $T_R \sim 10^{10}$ GeV, which is well compatible with thermal leptogenesis [74].

The relic abundance of the neutralino may also depend on flavour violating entries of the squark (or slepton) mass matrices. In Ref. [75] this has been studied for the case of minimal supergravity scenarios, where flavour violating couplings can modify the annihilation and coannihilation modes that enter the Boltzmann equation in the typical scenario with thermal production of neutralinos. Similar conclusions have been found for flavour non-diagonal entries in the leptonic soft matrices [76]. Flavour-violating effects are, of course, also present in the discussed cases of moduli or gravitino decay. A full study of their impact within this context is, however, clearly beyond the scope of this work.

6. CONCLUSION

In this paper, we have studied the consequences of non-minimal flavour violation in minimal anomaly-mediated supersymmetry breaking models, where tachyonic sleptons are avoided by introducing a common scalar mass similar to the one introduced in minimal supergravity. In these scenarios, new sources of flavour violation are in general introduced at high scales, leading to different flavour mixings for SM particles and their superpartners at the weak scale.

Using the conventional parameterization of squark mixing at the weak scale, we analyzed the viable AMSB parameter space in the light of the latest limits on low-energy observables and of the latest results from direct searches for Higgs and SUSY particles at the LHC. We found that intermediate values of $\tan\beta = 10\dots 30$ and relatively large scalar masses of $m_0 = 1\dots 3$ TeV, increasing with $\tan\beta$, were preferred and allowed for sizeable flavour violation in the left-left and essentially unconstrained flavour violation in the right-right squark sectors.

We completed our analytical calculations of flavour-violating supersymmetric particle production at hadron colliders with those related to gluino pair production and to the associated production of gluinos with charginos and neutralinos as well as with squarks. The corresponding cross sections were expected to be large due to the strong coupling of gluinos to the initial quarks and gluons. Flavour violation effects were expected to be only significant for the associated production of gluinos and squarks, since the other processes involved (almost) complete sums over internal squark exchanges.

This was confirmed in our numerical analysis for the high-energy phase of the LHC, where phenomena such as avoided crossings or smooth flavour dependences known from our previous studies could again be observed. For the experimental analysis of the ensuing cascade decays, leading to final states with second and third generation quarks and missing transverse energy, we referred the reader to previously published dedicated studies performed, *e.g.*, in supergravity models. The corresponding analysis in AMSB models was beyond the scope of this paper and is left for future work.

Finally, we briefly addressed the related cosmological aspects, showing that the well-known problem of dark matter underabundance in minimal AMSB models could be solved with moduli or gravitino decays also in the presence of flavour violation.

Acknowledgments

The authors would like to thank W. Porod for helpful discussions. This work has been supported by the Theory-LHC France-initiative of the CNRS/IN2P3 and by the ‘‘Helmholtz Alliance for Astroparticle Physics HAP’’ funded by the Initiative and Networking Fund of the Helmholtz Association.

-
- [1] H. P. Nilles, Phys. Rept. **110** (1984) 1.
 - [2] H. E. Haber and G. L. Kane, Phys. Rept. **117** (1985) 75.
 - [3] L. J. Hall, V. A. Kostelecky and S. Raby, Nucl. Phys. B **267** (1986) 415.
 - [4] G. Bozzi, B. Fuks, B. Herrmann and M. Klasen, Nucl. Phys. B **787** (2007) 1.
 - [5] B. Fuks, B. Herrmann and M. Klasen, Nucl. Phys. B **810** (2009) 266.
 - [6] A. H. Chamseddine, R. L. Arnowitt, P. Nath, Phys. Rev. Lett. **49** (1982) 970.
 - [7] R. Barbieri, S. Ferrara, C. A. Savoy, Phys. Lett. **B119** (1982) 343.
 - [8] M. Dine, W. Fischler and M. Srednicki, Nucl. Phys. B **189** (1981) 575;
S. Dimopoulos and S. Raby, Nucl. Phys. B **192** (1982) 353;
C. Nappi and B. Ovrut, Phys. Lett. B **113** (1982) 175.
 - [9] M. Dine and A. E. Nelson, Phys. Rev. D **48** (1993) 1277;
M. Dine, A. E. Nelson and Y. Shirman, Phys. Rev. D **51** (1995) 1362;
M. Dine, A. E. Nelson, Y. Nir and Y. Shirman, Phys. Rev. D **53** (1996) 2658.
 - [10] G. F. Giudice and R. Rattazzi, Nucl. Phys. B **511** (1998) 25;
N. Arkani-Hamed, G. F. Giudice, M. A. Luty and R. Rattazzi, Phys. Rev. D **58** (1998) 115005.
 - [11] G. F. Giudice and R. Rattazzi, Phys. Rept. **322** (1999) 419.
 - [12] K. Tobe, J. D. Wells and T. Yanagida, Phys. Rev. D **69** (2004) 035010.
 - [13] S. L. Dubovsky and D. S. Gorbunov, Nucl. Phys. B **557** (1999) 119.
 - [14] L. Randall, R. Sundrum, Nucl. Phys. **B557** (1999) 79-118.
 - [15] G. F. Giudice, M. A. Luty, H. Murayama *et al.*, JHEP **9812** (1998) 027.
 - [16] T. Gherghetta, G. F. Giudice, J. D. Wells, Nucl. Phys. **B559** (1999) 27-47.
 - [17] A. Pomarol, R. Rattazzi, JHEP **9905** (1999) 013.

- [18] I. Jack, D. R. T. Jones, Phys. Lett. **B465** (1999) 148-154.
- [19] N. Arkani-Hamed, D. E. Kaplan, H. Murayama *et al.*, JHEP **0102** (2001) 041.
- [20] J. L. Feng, T. Moroi, L. Randall *et al.*, Phys. Rev. Lett. **83** (1999) 1731-1734.
- [21] J. L. Feng, T. Moroi, Phys. Rev. **D61** (2000) 095004.
- [22] R. Rattazzi, A. Strumia, J. D. Wells, Nucl. Phys. **B576** (2000) 3-28.
- [23] A. J. Barr, C. G. Lester, M. A. Parker *et al.*, JHEP **0303** (2003) 045.
- [24] Z. Chacko, M. A. Luty, I. Maksymyk *et al.*, JHEP **0004** (2000) 001.
- [25] E. Katz, Y. Shadmi, Y. Shirman, JHEP **9908** (1999) 015.
- [26] I. Jack, D. R. T. Jones, Phys. Lett. **B482** (2000) 167-173.
- [27] I. Jack, D. R. T. Jones, Nucl. Phys. **B662** (2003) 63-88.
- [28] B. Murakami, J. D. Wells, Phys. Rev. **D68** (2003) 035006.
- [29] R. Kitano, G. D. Kribs, H. Murayama, Phys. Rev. **D70** (2004) 035001.
- [30] M. Ibe, R. Kitano, H. Murayama, Phys. Rev. **D71** (2005) 075003.
- [31] R. Hodgson, I. Jack, D. R. T. Jones *et al.*, Nucl. Phys. **B728** (2005) 192-206.
- [32] D. R. T. Jones, G. G. Ross, Phys. Lett. **B642** (2006) 540-545.
- [33] R. Hodgson, I. Jack, D. R. T. Jones, JHEP **0710** (2007) 070.
- [34] F. Gabbiani, E. Gabrielli, A. Masiero and L. Silvestrini, Nucl. Phys. B **477** (1996) 321.
- [35] B. C. Allanach, G. Hiller, D. R. T. Jones *et al.*, JHEP **0904** (2009) 088.
- [36] <https://twiki.cern.ch/twiki/bin/view/AtlasPublic/SupersymmetryPublicResults>
- [37] <https://twiki.cern.ch/twiki/bin/view/CMSPublic/PhysicsResultsSUS>
- [38] K. Nakamura *et al.* [Particle Data Group], J. Phys. G **37** (2010) 075021.
- [39] D. Asner *et al.* [Heavy Flavor Averaging Group], arXiv:1010.1589 [hep-ex].
- [40] J. S. Hagelin, S. Kelley and T. Tanaka, Nucl. Phys. B **415** (1994) 293.
- [41] P. Brax and C. A. Savoy, Nucl. Phys. B **447** (1995) 227.
- [42] M. Ciuchini, E. Franco, D. Guadagnoli, V. Lubicz, M. Pierini, V. Porretti and L. Silvestrini, Phys. Lett. B **655** (2007) 162.
- [43] T. Hurth, E. Lunghi and W. Porod, Nucl. Phys. B **704** (2005) 56.
- [44] M. Misiak *et al.*, Phys. Rev. Lett. **98** (2007) 022002.
- [45] T. Huber, T. Hurth and E. Lunghi, Nucl. Phys. B **802** (2008) 40.
- [46] CMS-PAS-BPH-11-019.
- [47] P. Ball and R. Fleischer, Eur. Phys. J. C **48** (2006) 413.
- [48] T. Moroi, Phys. Rev. D **53** (1996) 6565 [Erratum-ibid. D **56** (1997) 4424].
- [49] W. Porod, Comput. Phys. Commun. **153** (2003) 275.
- [50] ATLAS-CONF-2011-163.
- [51] CMS-PAS-HIG-11-032.
- [52] M. Lancaster [Tevatron Electroweak Working Group and for the CDF and D0 Collaborations], arXiv:1107.5255 [hep-ex].
- [53] B. C. Allanach, T. J. Khoo and K. Sakurai, arXiv:1110.1119 [hep-ph].
- [54] S. P. Martin, J. D. Wells, Phys. Rev. **D64** (2001) 035003.
- [55] B. C. Allanach *et al.*, Eur. Phys. J. C **25** (2002) 113.
- [56] T. Hurth and W. Porod, JHEP **0908** (2009) 087.
- [57] A. Bartl, K. Hidaka, K. Hohenwarter-Sodek, T. Kernreiter, W. Majerotto and W. Porod, Phys. Lett. B **679** (2009) 260.
- [58] A. Bartl, H. Eberl, B. Herrmann, K. Hidaka, W. Majerotto and W. Porod, Phys. Lett. B **698** (2011) 380 [Erratum-ibid. B **700** (2011) 390]
- [59] M. Bruhnke, B. Herrmann and W. Porod, JHEP **1009** (2010) 006.
- [60] A. Bartl, H. Eberl, E. Ginina, B. Herrmann, K. Hidaka, W. Majerotto and W. Porod, arXiv:1107.2775 [hep-ph].
- [61] C. Gross and G. Hiller, Phys. Rev. D **83** (2011) 095015.
- [62] W. Beenakker, R. Hopker, M. Spira and P. M. Zerwas, Nucl. Phys. B **492** (1997) 51.
- [63] T. Gehrmann, D. Maitre and D. Wyler, Nucl. Phys. B **703** (2004) 147.
- [64] J. Pumplin, D. R. Stump, J. Huston, H. L. Lai, P. Nadolsky and W. K. Tung, JHEP **0207** (2002) 012.
- [65] E. Komatsu *et al.* [WMAP Collaboration], Astrophys. J. Suppl. **192** (2011) 18.
- [66] C. H. Chen, M. Drees and J. F. Gunion, Phys. Rev. D **55** (1997) 330 [Erratum-ibid. D **60** (1999) 039901].
- [67] T. Moroi and L. Randall, Nucl. Phys. B **570** (2000) 455.
- [68] P. Gondolo, J. Edsjö, P. Ullio, L. Bergstrom, M. Schelke and E. A. Baltz, JCAP **0407** (2004) 008; P. Gondolo, J. Edsjö, P. Ullio, L. Bergstrm, M. Schelke, E.A. Baltz, T. Bringmann and G. Duda, <http://www.darksusy.org>.
- [69] S. Rajagopalan, arXiv:1010.3384 [hep-ph].
- [70] L. Covi, J. E. Kim and L. Roszkowski, Phys. Rev. Lett. **82** (1999) 4180.
- [71] L. Covi, H. B. Kim, J. E. Kim and L. Roszkowski, JHEP **0105** (2001) 033.
- [72] B. S. Acharya, G. Kane, S. Watson and P. Kumar, Phys. Rev. D **80** (2009) 083529.
- [73] J. Pradler and F. D. Steffen, Phys. Rev. D **75** (2007) 023509.
- [74] W. Buchmuller, P. Di Bari and M. Plumacher, Annals Phys. **315** (2005) 305.
- [75] B. Herrmann, M. Klasen and Q. Le Boulc'h, Phys. Rev. D **84** (2011) 095007.
- [76] D. Choudhury, R. Garani and S. K. Vempati, arXiv:1104.4467 [hep-ph].